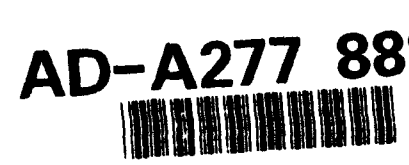

ARMY RESEARCH LABORATORY

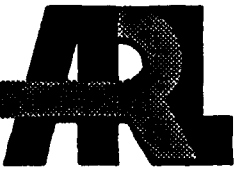

An Assessment of the Performance of the Original and Modified Versions of the Forest Fire Explosive Initiation Model

John Starkenberg

ARL-TR-373 March 1994

NOTICES

Destroy this report when it is no longer needed. DO NOT return it to the originator.

Additional copies of this report may be obtained from the National Technical Information Service, U.S. Department of Commerce, 5285 Port Royal Road, Springfield, VA 22161.

The findings of this report are not to be construed as an official Department of the Army position, unless so designated by other authorized documents.

The use of trade names or manufacturers' names in this report does not constitute indorsement of any commercial product.

REPORT DOCUMENTATION PAGE

Form Approved
OMB No. 0704-0188

1. AGENCY USE ONLY (Leave blank)	2. REPORT DATE	3. REPORT TYPE AND DATES COVERED
	March 1994	Final, 1 October 1991 - 30 September 1993

4. TITLE AND SUBTITLE

An Assessment of the Performance of the Original and Modified Versions of the Forest Fire Explosive Initiation Model

5. FUNDING NUMBERS

PR: 1L161102AH43

6. AUTHOR(S)

John Starkenberg

7. PERFORMING ORGANIZATION NAME(S) AND ADDRESS(ES)

U.S. Army Research Laboratory
ATTN: AMSRL-WT-TB
Aberdeen Proving Ground, MD 21005-5066

8. PERFORMING ORGANIZATION REPORT NUMBER

9. SPONSORING/MONITORING AGENCY NAME(S) AND ADDRESS(ES)

U.S. Army Research Laboratory
ATTN: AMSRL-OP-CI-B (Tech Lib)
Aberdeen Proving Ground, MD 21005-5066

10. SPONSORING/MONITORING AGENCY REPORT NUMBER

ARL-TR-373

11. SUPPLEMENTARY NOTES

12a. DISTRIBUTION/AVAILABILITY STATEMENT

Approved for public release; distribution is unlimited.

12b. DISTRIBUTION CODE

13. ABSTRACT (Maximum 200 words)

The Forest Fire explosive initiation model is useful because it can be calibrated from readily available sensitivity data. However, assumptions used in the Forest Fire derivation limit its accuracy and applicability. Present computations show that, while Forest Fire adequately predicts run to detonation for sustained-shock loading, it is grossly in error when applied to pulsed-shock loading. On the other hand, it exhibits some qualitatively correct results for finite-rate compression or ramp-wave loading. Several relatively simple modifications which extend the applicability of Forest Fire have been developed. These include improved mixture modeling, use of a higher order reactive Hugoniot to describe ignition, and incorporation of surface area burning into the reaction rate model. These modifications significantly affect the predicted response to pulsed-shock loading. Combining surface burning with a quadratic reactive Hugoniot provides a significantly improved representation of response to pulsed-shock stimulus.

14. SUBJECT TERMS	15. NUMBER OF PAGES
explosives, explosive initiation, shock initiation, models	48
	16. PRICE CODE

17. SECURITY CLASSIFICATION OF REPORT	18. SECURITY CLASSIFICATION OF THIS PAGE	19. SECURITY CLASSIFICATION OF ABSTRACT	20. LIMITATION OF ABSTRACT
UNCLASSIFIED	UNCLASSIFIED	UNCLASSIFIED	UL

INTENTIONALLY LEFT BLANK.

ACKNOWLEDGMENT

The author is grateful to Mrs. Kelly Benjamin for preparing many of the final figures for this report.

INTENTIONALLY LEFT BLANK.

TABLE OF CONTENTS

INTENTIONALLY LEFT BLANK.

LIST OF FIGURES

1. INTRODUCTION

"Forest Fire" is the first and simplest of a number of models treating the initiation of detonation in energetic materials (Mader 1970, 1979; Mader and Forest 1976; Lundstrom 1988). It is useful because it can be calibrated from readily available sensitivity data. The more recent models are increasingly sophisticated and capture more of the micromechanical phenomenology involved in initiation of heterogeneous explosives (Lee and Tarver 1980; Johnson, Tang and Forest 1985; Tang, Johnson and Forest 1985). Often, however, Forest Fire is the only choice available for a given energetic material. A problem arises in that, on the basis of the assumptions used in its derivation, Forest Fire is quite limited in its range of applicability. It can be expected to adequately predict the distance of run to detonation for sustained-shock loading as it is directly calibrated to do just that. However, in the complex environments associated with accidental initiation, pulsed-shock and finite-rate compression (or ramp-wave) loading is common (Starkenberg et al. 1989).

Indeed, Forest Fire is routinely employed in these environments, and beyond its limits(Bowman et al. 1981; Starkenberg, Huang and Arbuckle 1984; Cost et al. 1981). The consequences of this on the accuracy of the results achieved require clarification, as the literature does not include assessments of Forest Fire performance for pulsed shocks or ramp waves. The present report is, in part, an attempt to rectify this situation by comparing computational predictions with experimental results for sustained- and pulsed-shock loading of PBX-9404.

In the course of pursuing this understanding, it became clear that several relatively simple modifications might extend the applicability of Forest Fire. These modifications include improved mixture modeling, use of a more realistic reactive Hugoniot, and incorporation of surface area burning into the reaction rate model. These modifications not only improve the performance of the model but also serve to illustrate the sources of the shortcomings in the original Forest Fire model.

2. FOREST FIRE

A brief discussion of the Forest Fire model is included here to give necessary background. A more detailed exposition has been provided by Lundstrom (1988). Forest Fire may be considered to consist of a mixture model, a reactive shock model, and a reaction propagation model.

The two-phase reacting mixture has been characterized by the reactant mass fraction (which varies from 1 to 0 as reaction proceeds). However, the product mass fraction (which varies from 0 to 1) provides a more intuitive description and has been used in the present implementation. The reactant and product mass fractions are simply related. The phases are assumed to be in mechanical and thermal equilibrium; that is, they are assumed to have equal pressures and temperatures. Generally, the times required to achieve thermal equilibrium (via conduction) are significantly longer than those required to achieve mechanical equilibrium (via wave propagation). Therefore, the condition of mechanical equilibrium can be satisfied more often than the condition of thermal equilibrium. Also required are equations of state for each phase giving pressure and temperature as functions of density, and specific internal energy. Forest Fire makes use of the rather complicated "HOM" equations of state for solid reactants and gaseous products.

The reactive shock is described by a reactive Hugoniot, connecting the unreacted ambient state with the Chapman-Jouget state. This Hugoniot gives shock velocity as a linear function of particle velocity. While the reactive Hugoniot is a part of the Forest Fire derivation, and directly affects the reaction rate law, it is not generally used to describe reactive shock waves in hydrocode implementations where shock waves are modeled using artificial viscosity. In this case, the propagation rate law is integrated from the unreacted state through the distorted time scale associated with the viscous shock. The approach has low physical fidelity, and results are reported to be improved by including the artificial viscous stress along with the pressure in calculating the reaction rate. This has the effect of increasing the amount or reaction associated with the shock wave, which may be lower than that associated with the reactive Hugoniot. Specifically, this represents the method that has been implemented in the 2DE code (Kershner and Mader 1972; Mader 1979). During most of the development of a detonation, the amount of reaction associated with the shock is small, and the process is dominated by downstream reaction. The final transition to detonation occurs rapidly over a short distance. Thus, use of this technique can be expected to have little effect on predicted distances of run to detonation. In the present implementation, artificial viscosity is not employed, and the reactive Hugoniot is used explicitly. It should be emphasized that, although Forest Fire has no explicit ignition ("hot spot") step, the reaction associated with the shock wave, whether determined by integration or by the reactive Hugoniot, plays this role.

The empirical reaction rate law is derived assuming that bulk reaction takes place. That is, the reaction rate is proportional to the reactant mass fraction and "hot spots," and surface burning phenomena are specifically excluded. The pressure dependence is obtained with reference to the "Pop plot," which represents commonly available sensitivity data for high explosives (run distance to detonation as a function

of initial shock pressure) obtained in the "wedge test" (Ramsay and Popolato 1965). The "single curve build-up hypothesis" interprets the Pop plot as the path to detonation in the pressure-distance plane so that the solutions obtained automatically reproduce wedge test results. The derivation is simplified by assuming that the pressure gradient behind the shock vanishes. This condition is met only when the shock-wave transitions to detonation as a growing square wave. The derived Forest Fire rate is a function of the state variables immediately downstream of the shock wave. This is fitted as a function of pressure and applied at all points downstream of the shock. It is a peculiarity of this fit that the rate is not defined for pressures above the Chapman-Jouget value. The original fit is a polynomial in pressure of as many as fifteen terms.

3. COMPUTATIONAL METHODS

Computations were made using the One-Dimensional Explicit Shock (ODES) code (Starkenberg 1989). The use of a one-dimensional code naturally limits the study to consideration of one-dimensional phenomena. However, this is quite sufficient to cover response to sustained-shock, pulsed-shock, and ramp-wave loading.

The most significant feature of ODES is its explicit modeling of shock waves. This approach is appropriate whenever the flow between the upstream and downstream states is quasi-steady. Generally, mass, momentum, and energy conservation along with overtaking characteristic compatibility, and other appropriate conditions are solved for downstream conditions with upstream conditions given. The shock waves thus treated may be either inert or reactive. In a reactive shock, some degree of reaction is associated with the shock jump. This eliminates the requirement to numerically resolve those parts of the reactive flow field which may satisfy the quasi-steady condition, and be concentrated in a narrow region downstream of the shock. In the case of a Chapman-Jouget detonation, the entire reactive flow field is unresolved. However, it should be noted that such spatial concentration does not guarantee that the quasi-steady condition is met. In conjunction with the Forest Fire model, the reactive Hugoniot is used to close the system of equations describing the shock wave, and is directly responsible for determining the amount of reaction associated with the shock.

Shock waves may be permitted to transition to reactive shock waves, and reactive shock waves to Chapman-Jouget or overdriven detonations. In addition to shock waves, ODES also gives explicit treatment to gradient discontinuities (such as the heads and tails of isentropic waves), and allows them to transition to shock waves. This is useful for modeling finite-rate compressions.

ODES produces three different plotting files. Boundary plots which show the positions of gradient discontinuities, shock waves, reactive shock waves, detonations, contact discontinuities (material interfaces), and pistons may be obtained. Profiles of density, internal energy, velocity, mass fraction, and numerous other variables as functions of position at various times are available. Histories of pressure and velocity at specified Lagrangian stations may also be produced.

4. FOREST FIRE PERFORMANCE

4.1 Sustained-Shock Stimulus. Sustained-shock computations were made using a "thick" (semi-infinite) copper flyer impacting a thick PBX-9404 sample to produce the stimulus. The velocity of the flyer was varied to produce different initial shock pressures.

One such computation was made with a flyer velocity of 550 m/s. The boundary plot in Figure 1 shows the positions of the shock wave propagating into the copper flyer, the interface between the copper and the PBX-9404, and the reactive shock propagating into the PBX-9404 sample as functions of time. Transition to detonation is evidenced by a change in the slope of the reactive shock. Figure 2 shows pressure profiles at various times. An approximation to a growing square wave prevails during most of the build-up process. This stands in contrast to results predicted by other models (Lee and Tarver 1980; Johnson, Tang, and Forest 1985; Starkenberg 1989) where transition to detonation occurs when a reaction-driven secondary compression overtakes the initial shock wave. The predicted pressure histories at several Lagrangian stations, shown in Figure 3, exhibit poor agreement with experimental measurements (Wackerle et al. 1978). Two related aspects of the computed results merit attention. First, the shock pressures are too high, and the shock propagates too rapidly. Since shock waves are treated explicitly here, the linear reactive Hugoniot determines the amount of reaction in the shock, which may be too great. Second, reaction proceeds too promptly following shock passage. It appears that improvement might be obtained by incorporating a model to delay reaction.

Predicted distances of run and times to detonation plotted as functions of initial shock pressure are compared with experimental data in Figures 4 and 5, respectively. Forest Fire was derived to predict the distance of run to detonation as a function of initial pressure (or Pop plot), and it is no surprise that it does this well (although the slope of the computed Pop plot differs somewhat from the experimental value [Gibbs and Popolato 1990]).

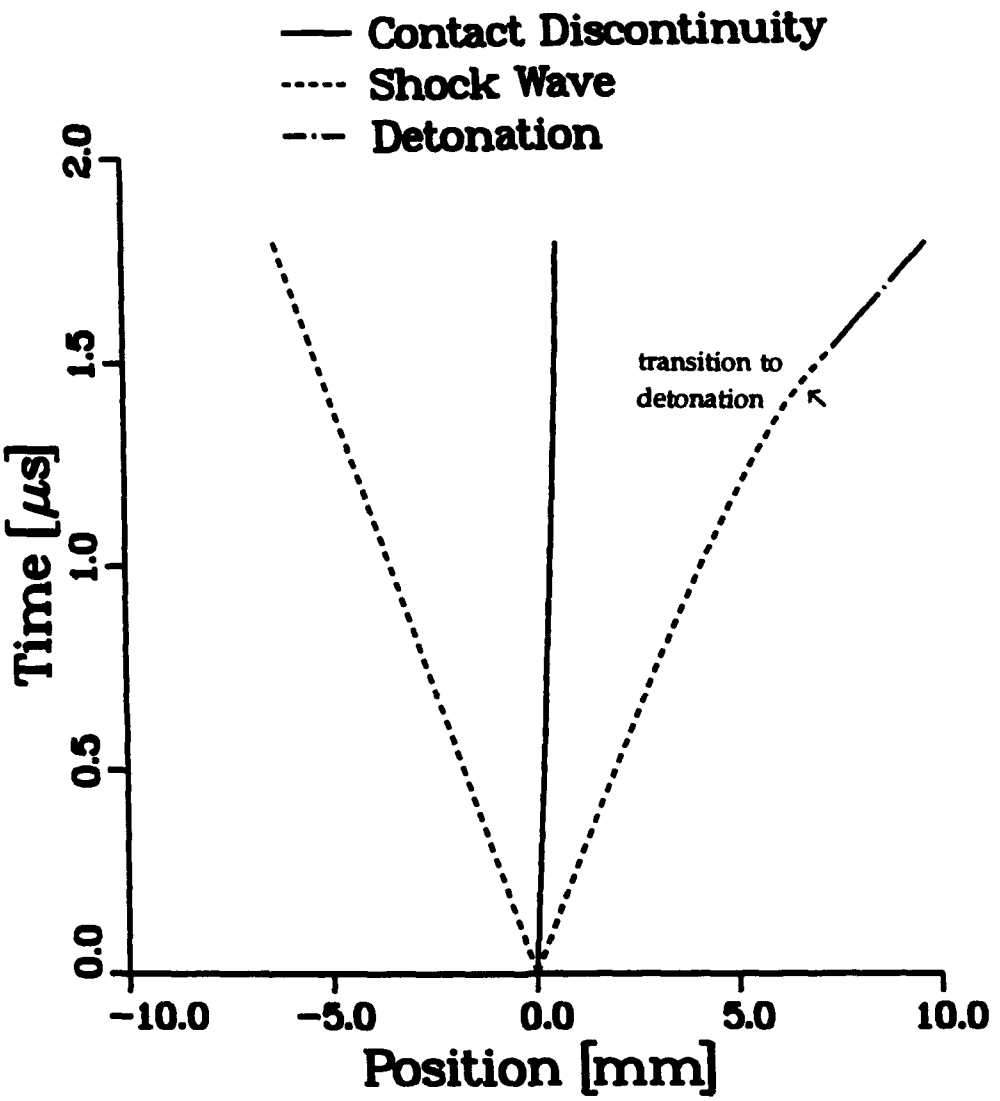

Figure 1. Boundary plot for the impact of a thick copper flyer on a PBX-9404 sample at 550 m/s showing the positions of the shock wave propagating into the flyer, the interface between the flyer and the sample, and the reactive shock propagating into the sample as functions of time. Transition to detonation is evidenced by a change in slope of the reactive shock.

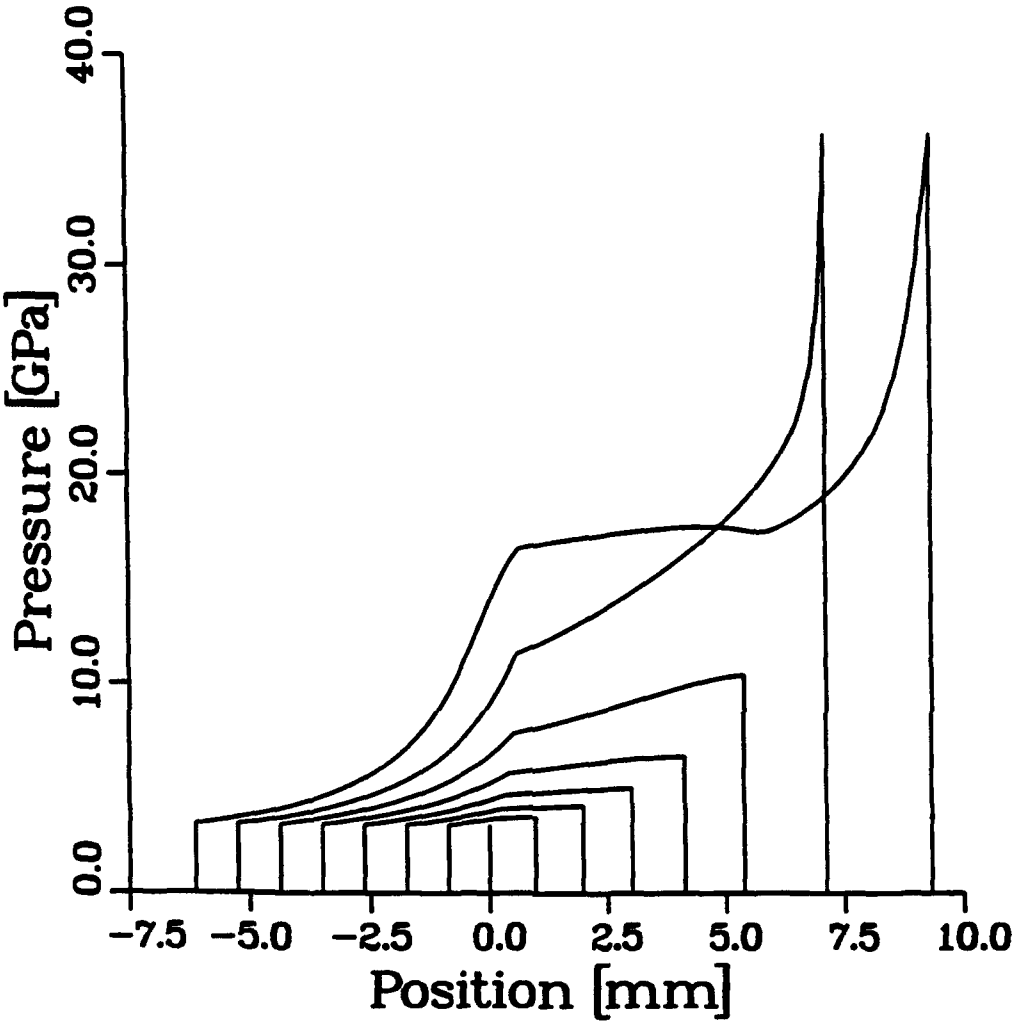

Figure 2. Sequence of pressure profiles showing detonation development in a PBX-9404 sample following the impact of a thick copper flyer at 550 m/s. The shock-wave transitions to detonation as a growing square wave.

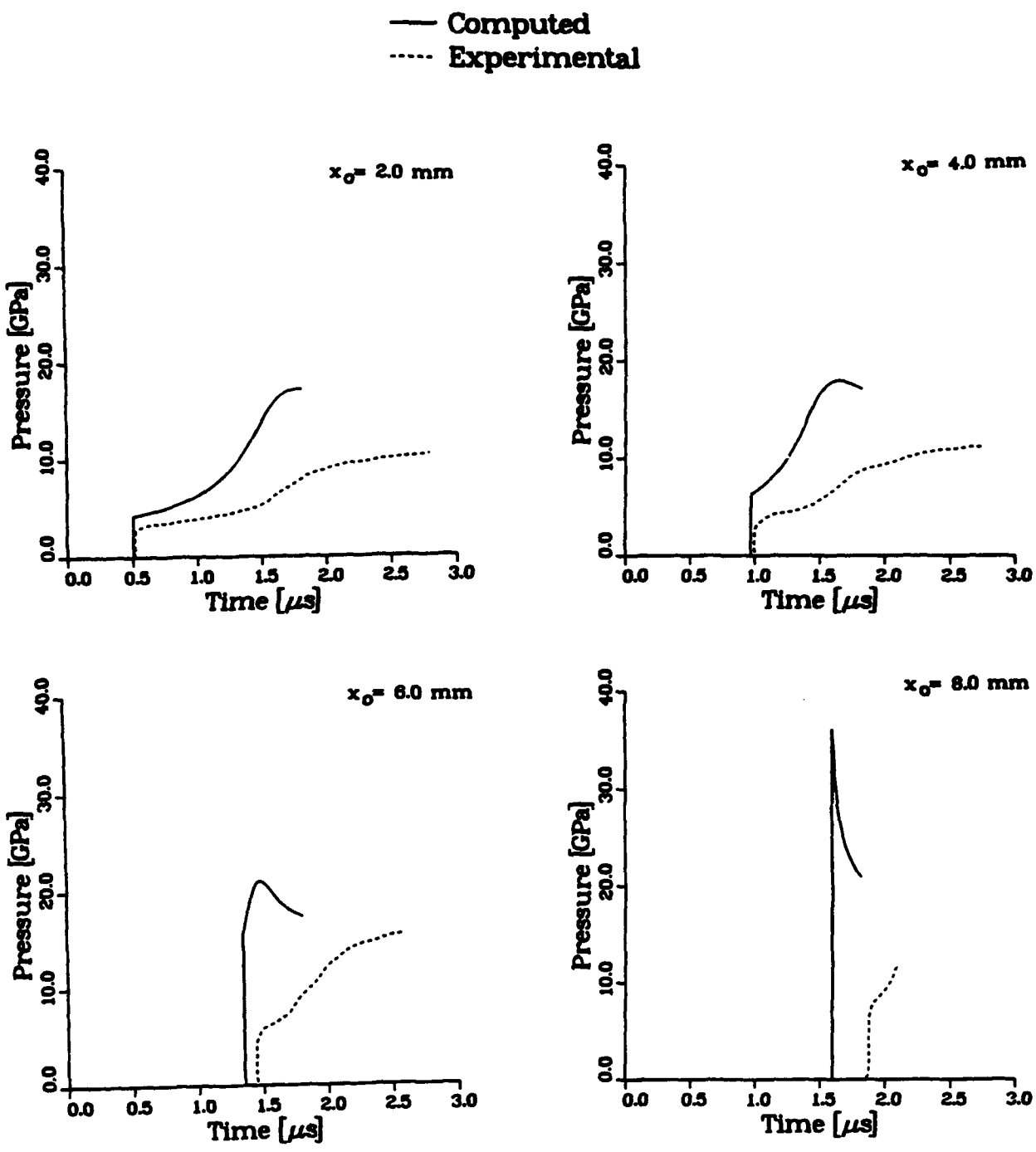

Figure 3. Comparison of experimental pressure histories with Forest Fire predictions at four Lagrangian stations following the impact of a thick copper flyer on a PBX-9404 sample at 550 m/s. The computed shock wave appears to incorporate too much reaction.

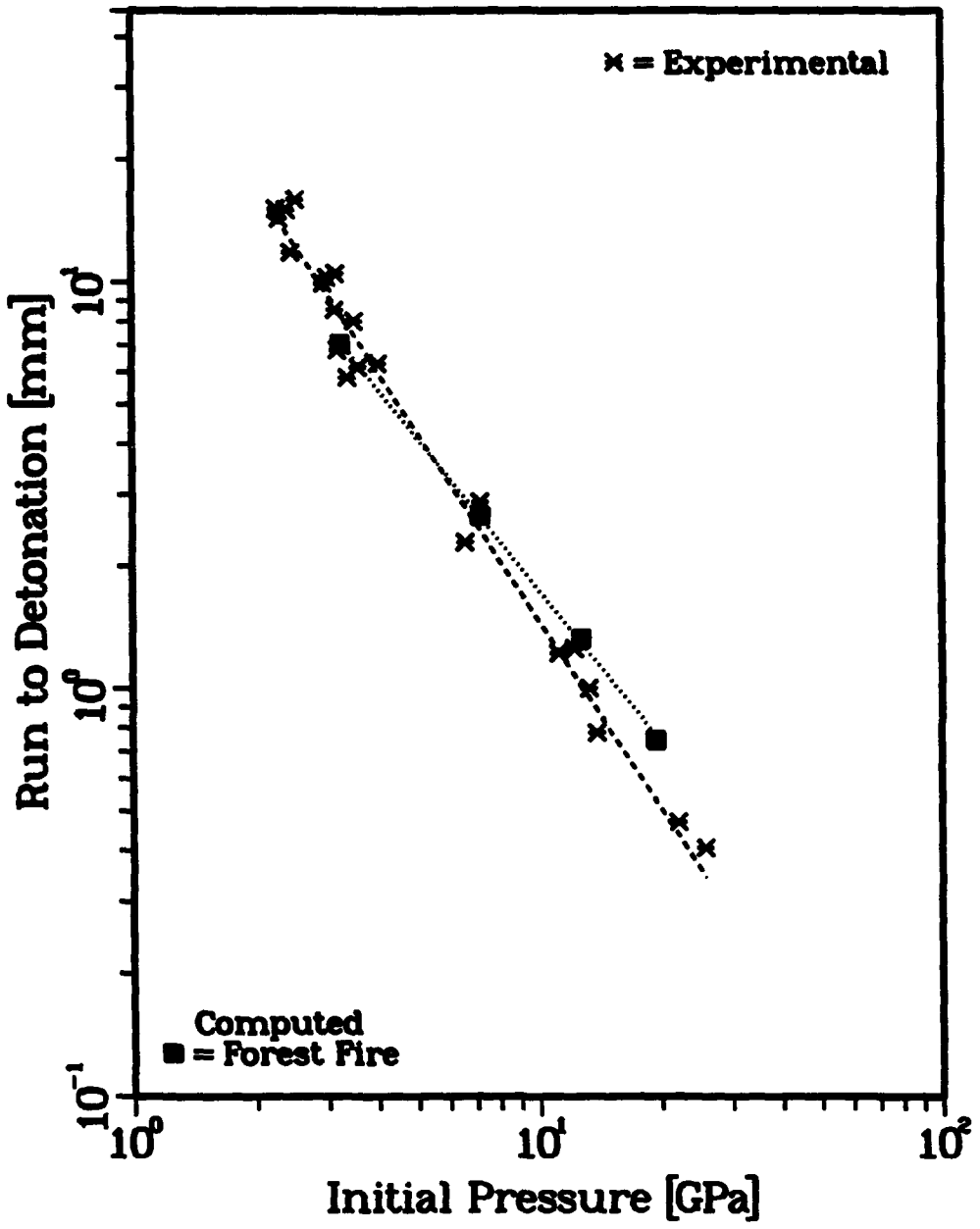

Figure 4. Comparison of the experimental run to detonation versus initial shock pressure with Forest Fire predictions for PBX-9404. The slope of the computed Pop plot differs somewhat from the experimental slope.

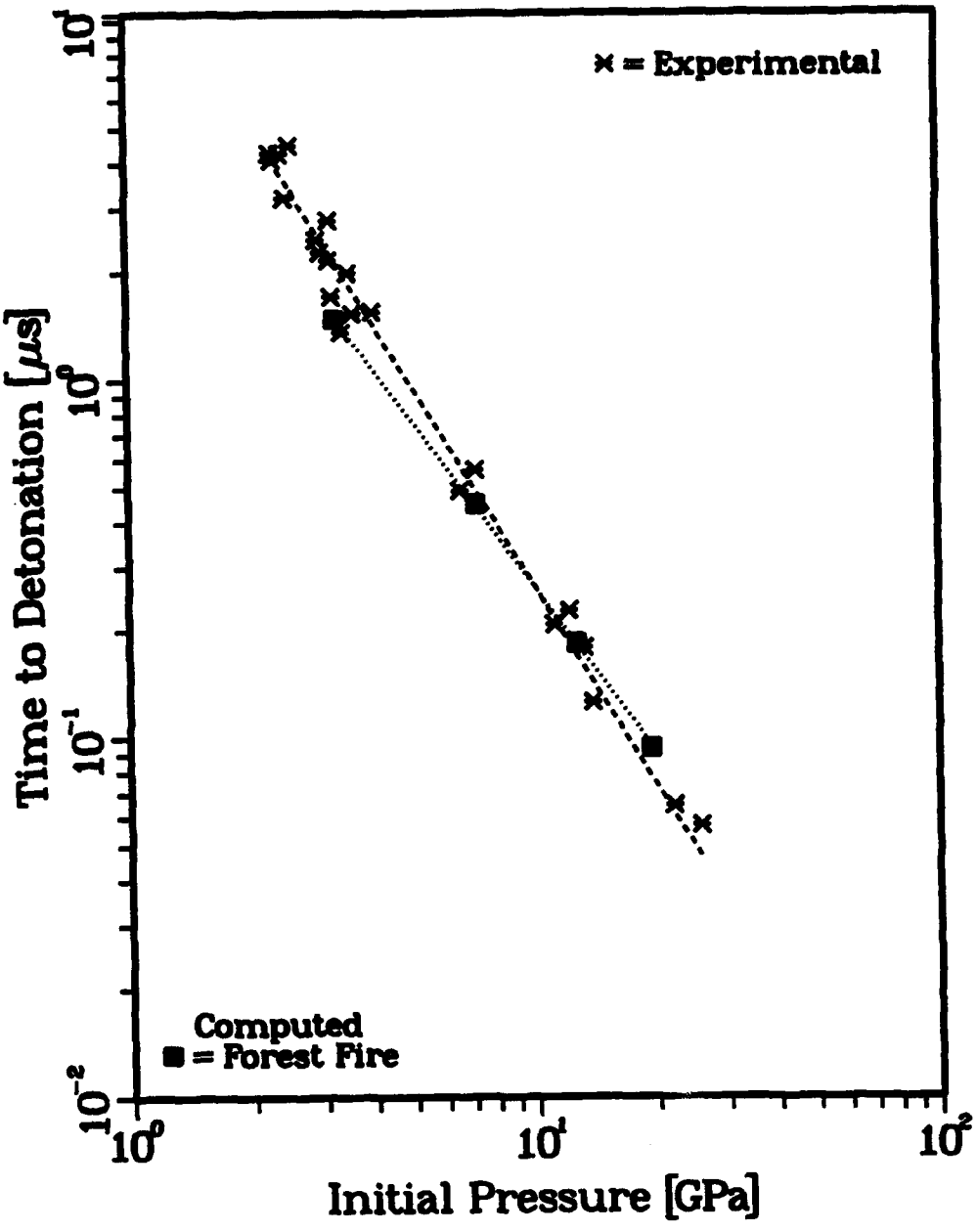

Figure 5. Comparison of the experimental time to detonation versus initial shock pressure with Forest Fire predictions for PBX-9404. The slope associated with the computed results differs somewhat from that associated with the experiments.

4.2 Pulsed-Shock Stimulus. Experimental data for the critical impact of thin mylar flyers on19.1-mm-thick PBX-9404 samples are fit well by a straight line in a log-log plot of flyer velocity versus flyer thickness (Weingart et al. 1984). This is shown in Figure 6. The critical velocities computed using Forest Fire correspond to transition to detonation occurring after 19.1 mm of run. They differ grossly from the experimentally determined values. The predicted sensitivity is much too high, and the variation appears slightly nonlinear for the thickest flyers.

In the experimental study by Wackerle, Rabie, Ginsberg, and Anderson (1984), pressure histories were also measured for a thin copper flyer impacting a PBX-9404 sample at the same 550-m/s velocity. Comparisons of the pressures measured at several stations with results from the corresponding numerical simulation are shown in Figure 7. Again, the shock pressures are too high, and reaction proceeds too promptly following shock passage. This is sufficient to negate the quenching effects of the rarefactions. The resulting error is biased toward safety when Forest Fire is used to predict initiation hazards. That is, Forest Fire predicts initiations that are not expected to occur.

4.3 Ramp Wave Stimulus. An experimental study of the response of an explosive to ramp waveswas conducted by Setchell (1981). In this study, the desired loading was produced by the impact of a copper flyer on a pyroceram layer covering a PBX-9404 sample. The constitutive nature of pyroceram causes the impact shock wave to disperse into a compression wave having a finite rise time. The rise time can be controlled by adjusting the thickness of the pyroceram cover. In these experiments, evidence of reaction increased as the rise time decreased. However, the effect on the run or time to detonation was not determined. Because a constitutive model for pyroceram was not readily available, the experiments were not directly simulated. However, ramp waves were generated computationally by specifying the pressure history at a boundary (piston) which is free to move accordingly.

Two such computations were made to assess the response of Forest Fire to ramp waves. In the first of these, boundary conditions corresponding to a linear pressure increase from ambient to a final value of 5.0 GPa over an interval of 1.0 μs were applied. In the second, the interval was cut in half. In each case, the boundary pressure was maintained at 5.0 GPa after reaching that value. For comparison, another computation was made in which a pressure-step boundary condition was used to produce a shock wave of the same strength.

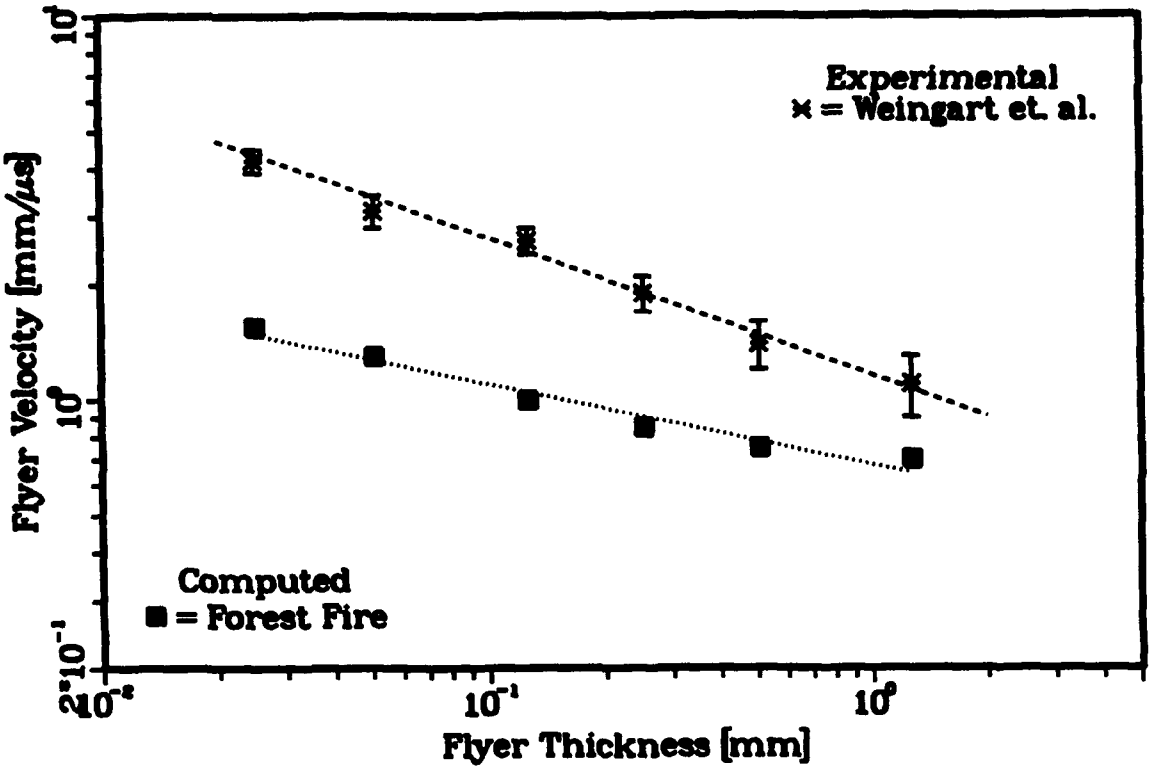

Figure 6. Comparison of experimental critical flyer velocity versus flyer thickness with Forest Fire predictions for initiation of PBX-9404 samples by thin mylar flyers. The predictions differ substantially from the experimental results.

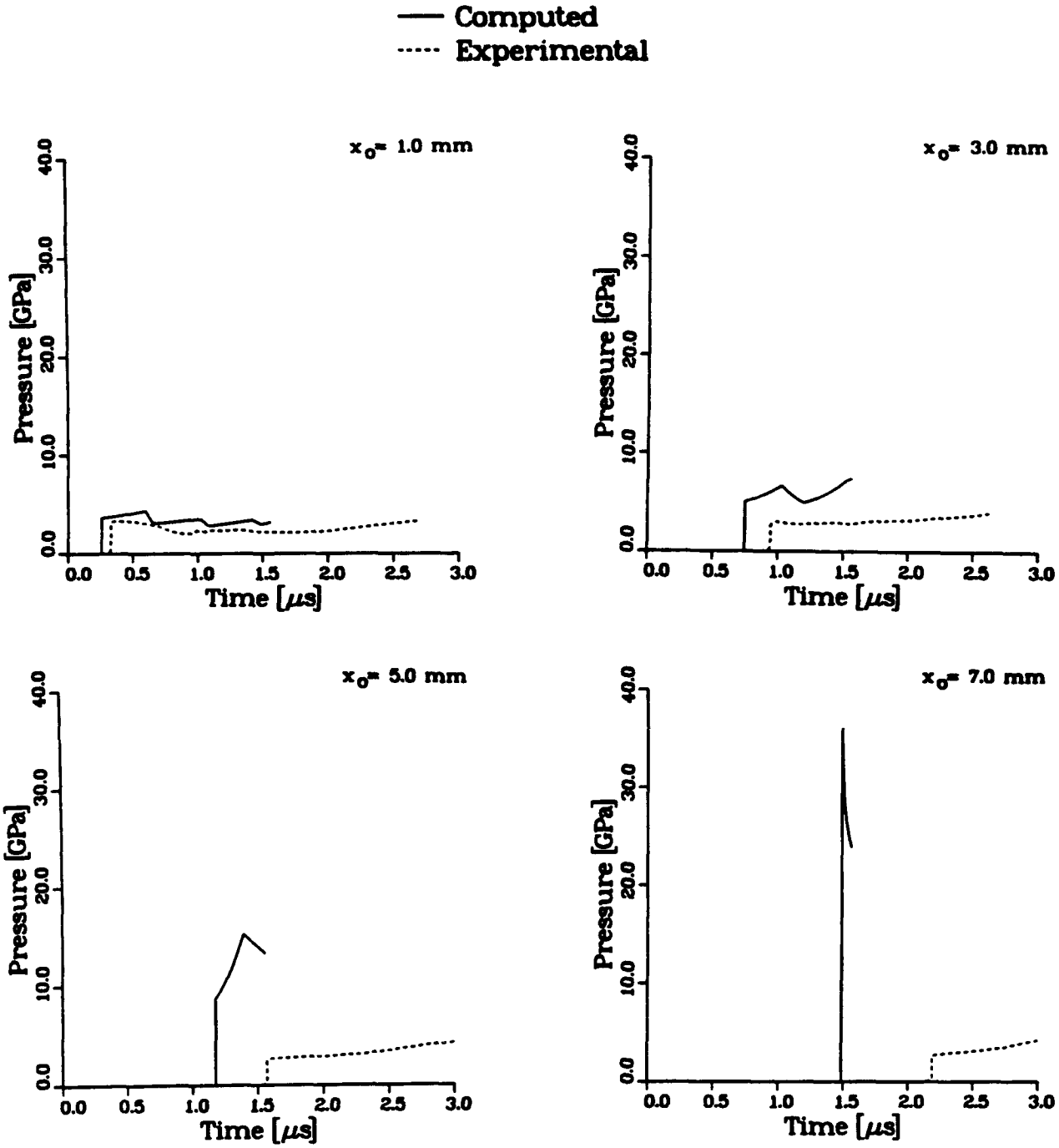

Figure 7. Comparison of experimental pressure histories with Forest Fire predictions at four Lagrangian stations following the impact of a 0.76-mm-thick copper flyer on a PBX-9404 sample at 550 m/s. The computed shock wave appears to incorporate too much reaction leading to rapid downstream reaction.

Figure 8 is a boundary plot comparing the wavefront positions in the three computations. The piston trajectories appear at the left side of the plot. Distinct line styles are used for isentropic waves, shock waves (inert and reactive), and detonations. The initial slopes of the ramp wave trajectories are the same, and correspond to the isentropic wave speed in the undisturbed explosive. The isentropic waves transition to inert shock waves, reactive shock waves, and finally to detonations. A detonation is shown only when reaction in the shock wave is complete. However, for practical purposes, transition to detonation is identified as the point at which the slope of the shock trajectory assumes the value associated with the detonation velocity (at which point reaction is nearly complete) rather than the point at which the line style changes. The times to detonation behave in the expected fashion qualitatively. The shock-wave transitions to detonation earliest, while the ramp waves transition first to reactive shock waves and then to detonations in order of increasing rise time. However, the distances of run to detonation for the shock and fast ramp appear virtually identical, while the run distance for the slow ramp is longest. The effect on the times to detonation is stronger than the effect on the run distances. Pressure histories at several stations are shown in Figure 9. These indicate that the fast ramp has transitioned to detonation at a 4.0-mm run while the shock wave has not.

While the computed results are, at least in part, qualitatively consistent with the observations of Setchell, their predictive accuracy cannot be assessed. Indeed, close correspondence to experimental results should not be anticipated if the effect of rise time variation is on the production of hot spots, a mechanism which is not included in Forest Fire. Lower predicted sensitivity to ramp waves is merely a reflection of the fact that no shock wave ignites the explosive, and, as the rise time increases, the explosive resides at lower pressures for longer periods. This result should be produced by any model in which reaction rate is a monotonically increasing function of pressure.

5. MODIFICATIONS

It is of interest to consider several modifications to the Forest Fire assumptions and resulting model. These include replacing thermal equilibrium with adiabatic reaction, changing the Hugoniot describing the reactive shock wave, and replacing bulk reaction with surface burning. Each of these modifications has been implemented without change in the pressure dependence of the reaction rate law.

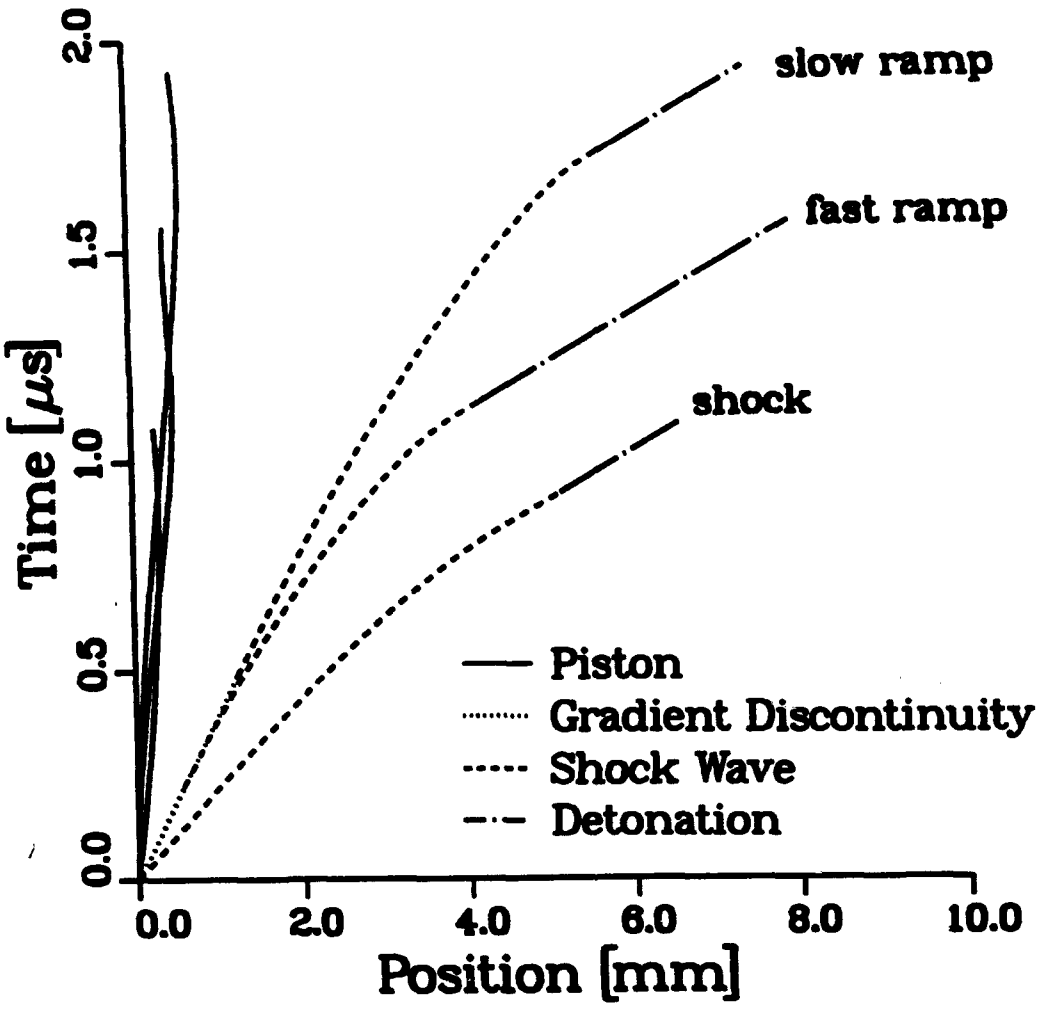

Figure 8. Comparison of predicted paths to detonation for PBX-9404 samples subjected to "slow-ramp," "fast-ramp," and shock-wave compressions. Transition to detonation is identified as the point at which the slope of the shock trajectory assumes the value associated with the detonation velocity and not where the line style changes. The times to detonation increase with increasing rise time but the run to detonation is shortest for the fast ramp.

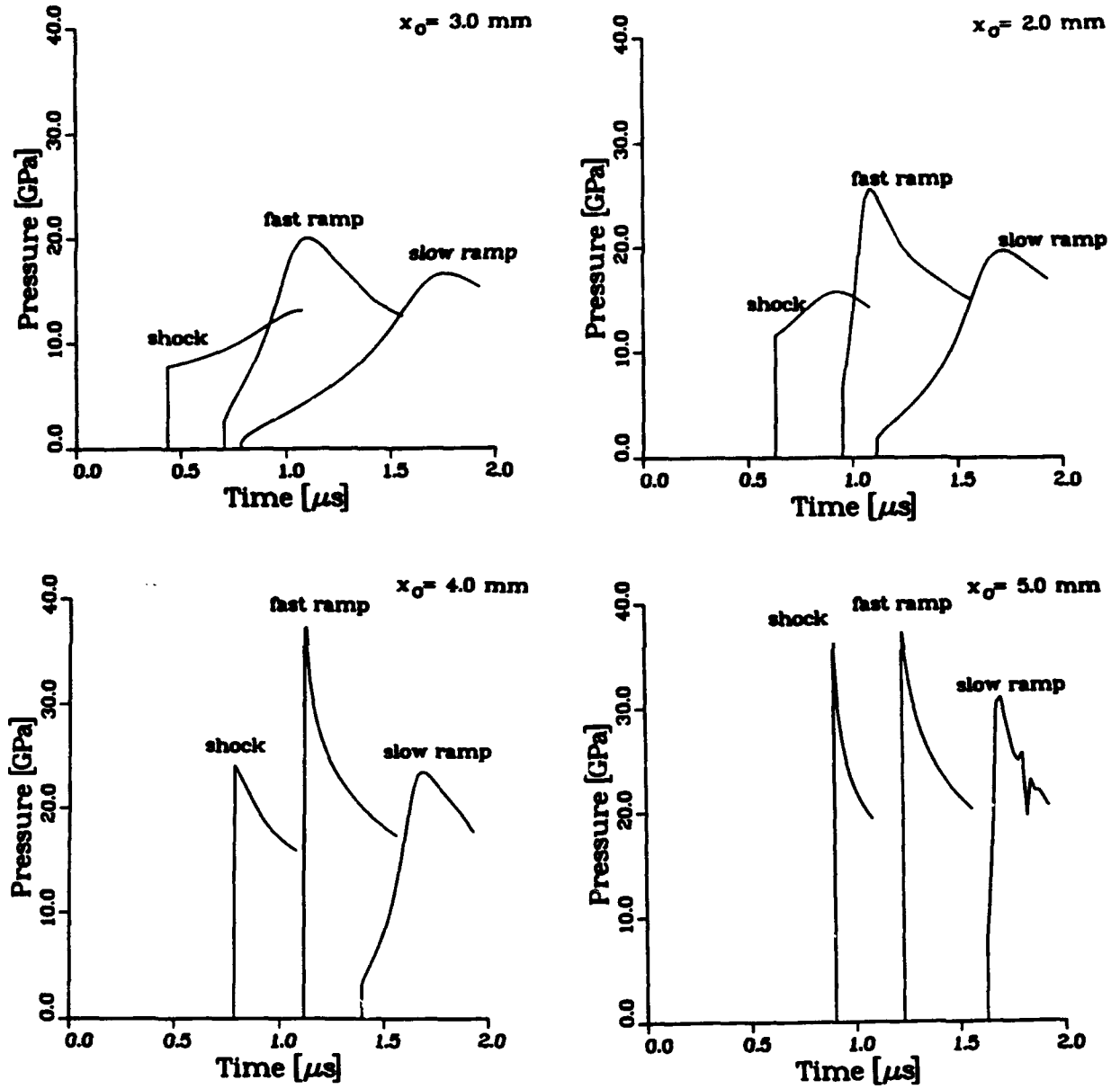

Figure 9. Comparison of predicted pressure histories at four Lagrangian stations for PBX-9404 subjected to "slow-ramp," "fast-ramp," and shock-wave compressions. The fast ramp produces the highest pressures.

5.1 Mixture Modeling. Forest Fire has been derived assuming that the reactant and product phases are in mechanical and thermal equilibrium. While the mechanical equilibrium assumption is generally plausible, thermal equilibrium has long been recognized as unrealistic (Lee and Tarver 1980; Johnson, Tang, and Forest 1985). The conditions of mechanical and thermal equilibrium in conjunction with known equations of state for each of the phases are sufficient to define an equation of state for the reacting mixture from which mixture pressure, and phase densities and internal energies may be determined as functions of mixture density and internal energy and product mass fraction in an iterative procedure. This may be functionally expressed as

$$p = p(\rho, e, y) \ ,$$

$$\rho_r = \rho_r(\rho, e, y) \ ,$$

$$e_r = e_r(\rho, e, y) \ ,$$

$$\rho_p = \rho_p(\rho, e, y) \ ,$$

and

$$e_p = e_p(\rho, e, y) \ ,$$

where the subscripts r and p refer to reactants and products respectively and unsubscripted variables refer to the mixture. Here, the product mass fraction, y, is used instead of the original reactant mass fraction, $1-y$, because its progression from 0 to 1 as reaction progresses provides a more natural description of the process.

An alternative has been offered in conjunction with the JTF initiation model which substitutes an isentropic reactant condition for thermal equilibrium (Johnson, Tang, and Forest 1985). This approach allows the given form of the mixture equation of state to be retained but suffers from the disadvantages of requiring time-consuming iterative integration of the isentrope equation as well as advection of the initial state along the isentrope throughout the flow field. Further, this formulation is limited to a particular form of the reactant equation of state.

If the partial differential equation describing conservation of energy of the mixture is split between the phases such that thermal isolation of the reactant phase (adiabatic reaction) is imposed, both the

reactant and product internal energies may be determined in the primary integration. For one-dimensional flow, the energyconservation equations for the mixture, and each phase are

$$\frac{\partial e}{\partial t} + u\frac{\partial e}{\partial x} + \frac{p}{\rho}\frac{\partial u}{\partial x} = h_d \dot{y}$$

$$\frac{\partial e_r}{\partial t} + u\frac{\partial e_r}{\partial x} + \frac{p}{\rho_r}\frac{\partial u}{\partial x} = 0$$

$$\frac{\partial e_p}{\partial t} + u\frac{\partial e_p}{\partial x} + \frac{p}{\rho_p}\frac{\partial u}{\partial x} = (e_r + h_d - e_p)\frac{\dot{y}}{y} \quad .$$

Note that the chemical energy released is treated as a potential energy of the reactants so that h_d is a positive constant and e represents the thermal component of the internal energy. Since the mixture and phase internal energies are related by a saturation condition, only two of the foregoing equations are needed in a computational implementation.

In this case, the mixture equation of state must give the mixture pressure and phase densities as functions of mixture density, phase internal energies, and product mass fraction:

$$p = p(\rho, e_r, e_p, y) \quad ,$$

$$\rho_r = \rho_r(\rho, e_r, e_p, y) \quad ,$$

and

$$\rho_p = \rho_p(\rho, e_r, e_p, y) \quad .$$

This can be achieved assuming only mechanical equilibrium in conjunction with the phase equations of state, which may have any form.

The effect on the pressure histories in the case of a 550-m/s thick copper flyer is shown in Figure 10. Results obtained under the adiabatic reaction assumption differ significantly from those obtained under the thermal equilibrium assumption at several stations. Adiabatic reaction produces a shorter run to detonation.

The effect on the Pop plot is shown in Figure 11. There is a small reduction in the predicted run distance. This does not significantly alter the quality of the agreement with the experiments.

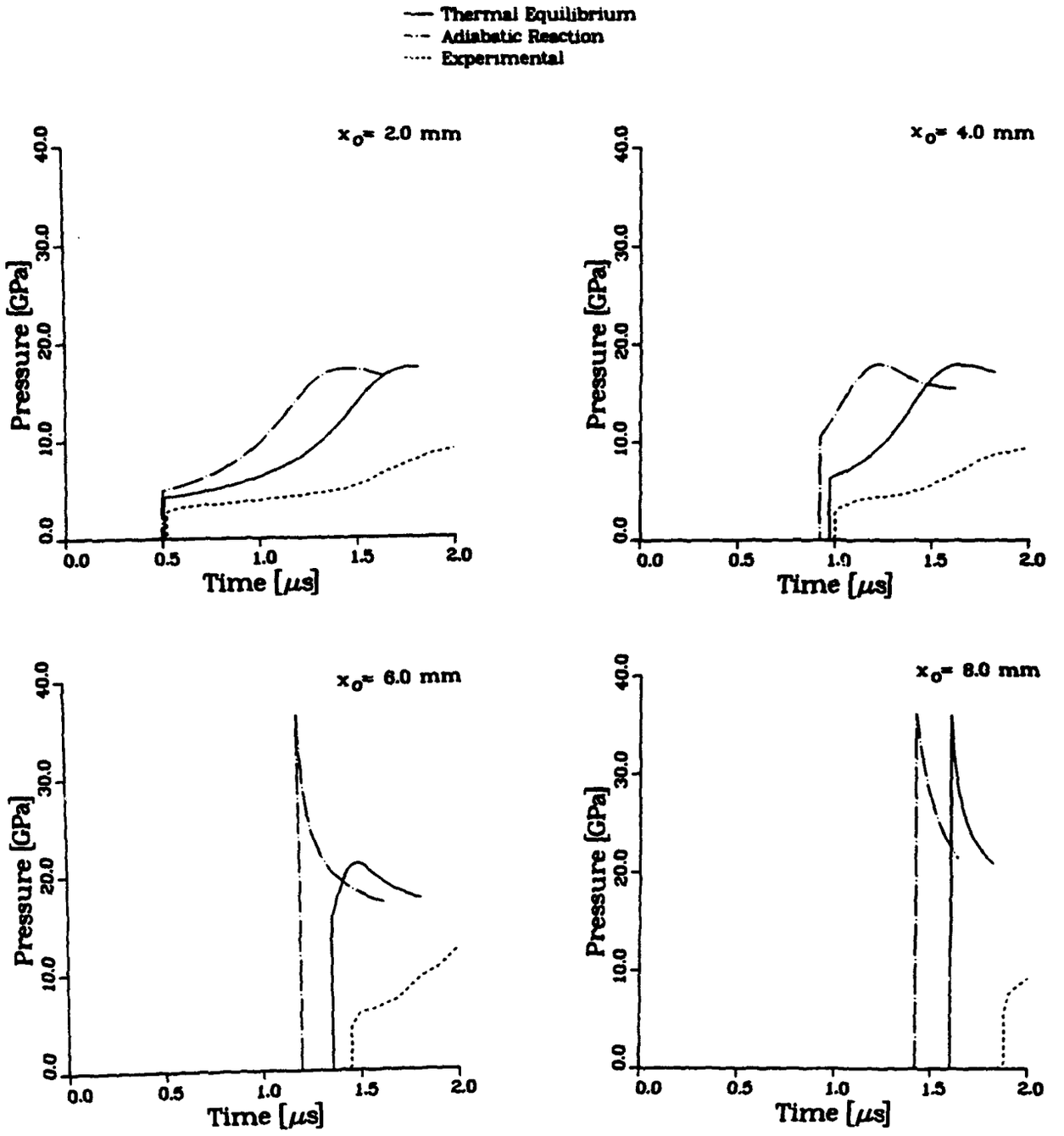

Figure 10. Effect of the mixture model on the predicted pressure histories in a PBX-9404 sample at four Lagrangian stations following the impact of a thick copper flyer at 550 m/s. Adiabatic reaction produces faster downstream reaction.

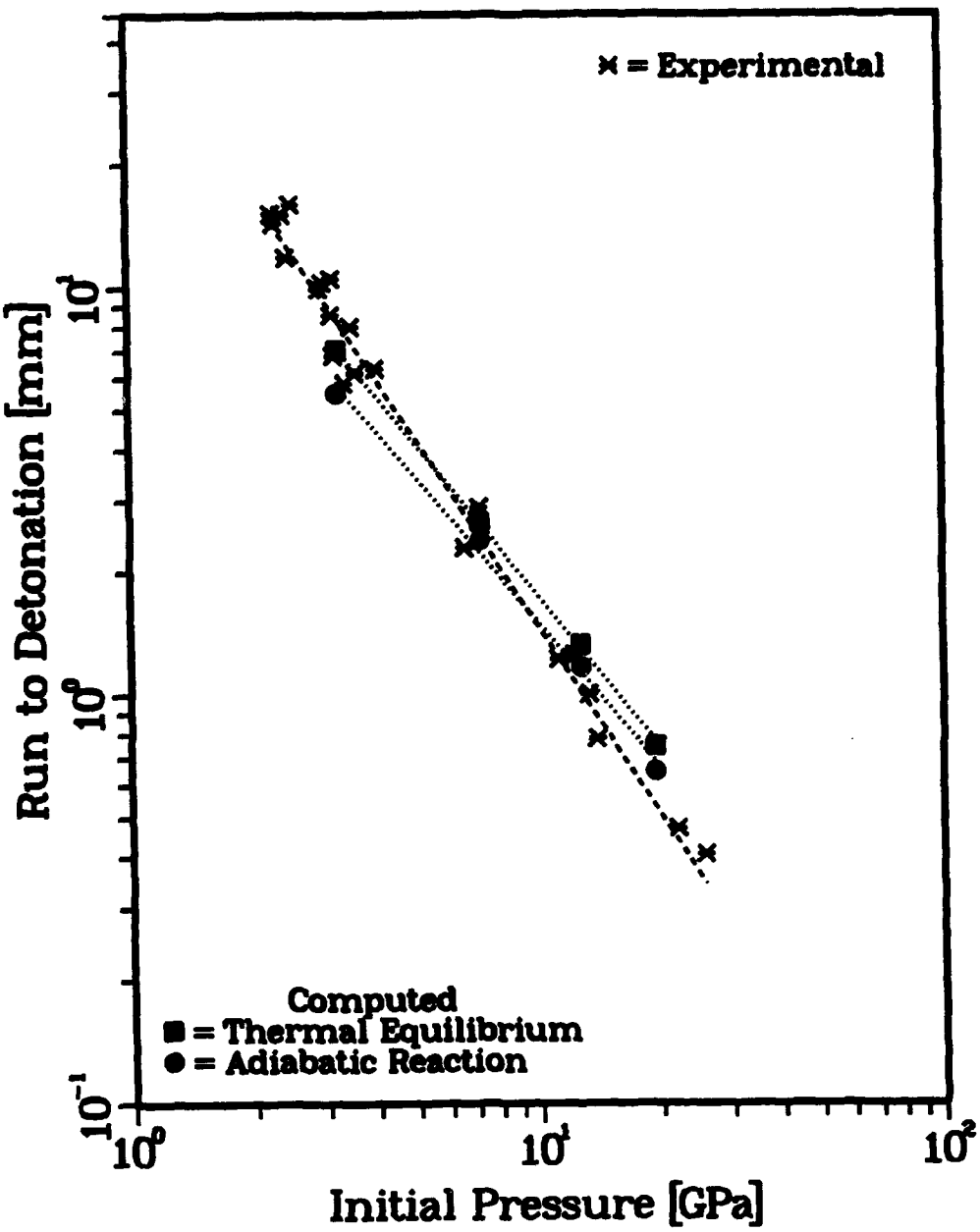

Figure 11. Effect of the mixture model on the predicted Pop plot of PBX-9404. The Pop plot is shifted toward slightly shorter runs with adiabatic reaction.

The effect on the response to pulsed shock waves is shown in Figure 12. There is a substantial reduction in the predicted critical flyer velocities which yields poorer agreement with experiments.

Because of the way Forest Fire is calibrated, agreement with experimental data is better when using the original model. *This should not be construed to imply that thermal equilibrium is in any way a superior assumption.* Since the mixture equation of state is used in the determination of the Forest Fire reaction rate coefficients, strictly speaking, these coefficients should be redetermined any time the equation of state is changed. However, the present computations were made to determine the effect of the mixture model with a fixed reaction rate law.

5.2 Reactive Shock-Wave Modeling. In the present implementation, the reactive Hugoniot is used to close the system of equations describing the reactive shock wave. It effectively determines the amount of reaction in the shock. As such, it constitutes Forest Fire's ignition model. The reactive Hugoniot also plays a role in determining the Forest Fire reaction rate. This role has not been considered, and the reaction rate is treated as a fixed property of the explosive as the reactive Hugoniot is varied.

The use of an inert shock in conjunction with the Forest Fire model, as suggested by Lundstrom (1988), was not considered advantageous. This would require numerical resolution of the entire reactive flow field. At least some portion of the reactive region may have a scale significantly smaller than that of the total flow field, and its resolution may carry a significant computation-time penalty. Use of a reactive shock wave becomes more advantageous as the shock approaches detonation, and includes greater levels of reaction.

The inert shock Hugoniot for the reactants is given by

$$U=c_i+s_i u \quad .$$

Forest Fire is derived using a linear reactive Hugoniot which connects the ambient state to the Chapman-Jouget state.

$$U=c_i+s_r u \quad ,$$

where

$$s_r=(D_{cj}-c_i)/u_{cj} \quad .$$

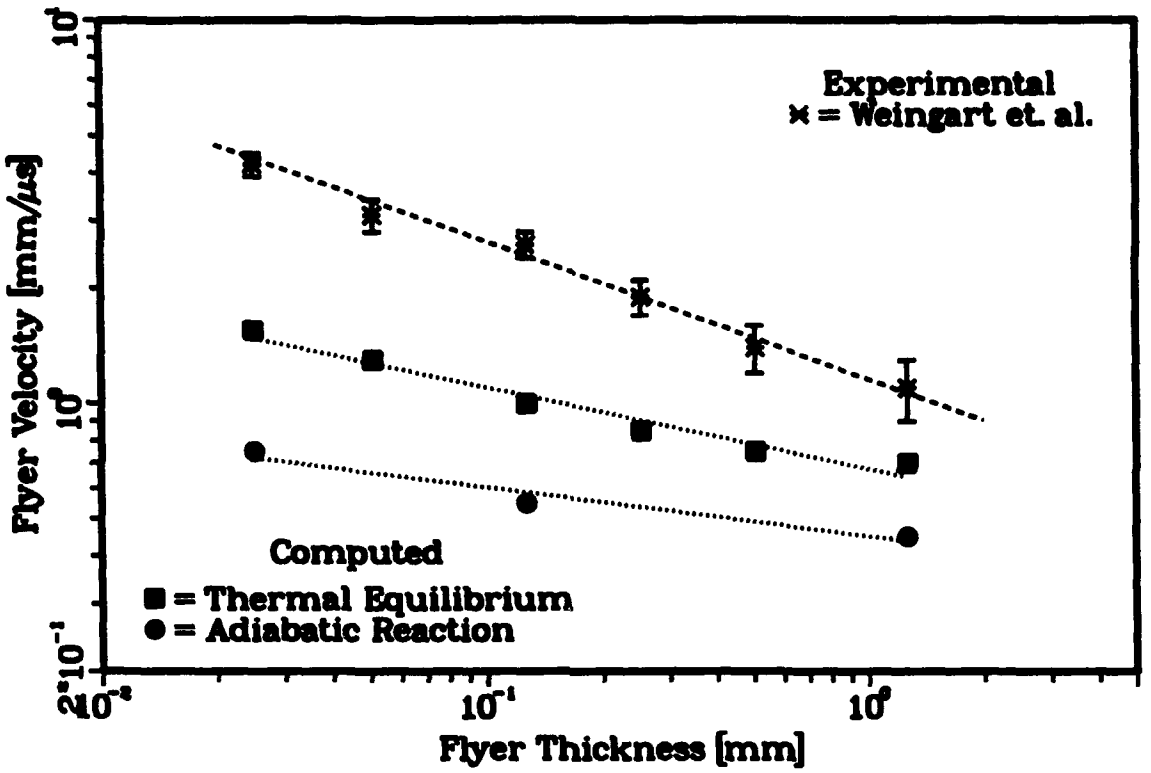

Figure 12. Effect of the mixture model on critical flyer velocities for initiation of PBX-9404 samples by thin mylar flyers. The critical velocity curve is shifted toward lower velocities.

The results computed using Forest Fire exhibit a level of reaction in low pressure shock waves which is too great to be consistent with experimental observations. More realistic representations are provided by higher order reactive Hugoniots which are initially tangent to the inert shock Hugoniot, and depart more gradually from inert behavior before approaching the Chapman-Jouget state. For example,

$$U=c_i+s_iu+s_nu^n \quad ,$$

where

$$s_n=[(D_{cj}-c_i)/u_{cj}-s_i]/u_{cj}^{n-1} \quad .$$

The linear and quadratic (n=2) reactive Hugoniots are illustrated in Figure 13 along with the inert Hugoniot.

The reactive Hugoniot appears explicitly in the Forest Fire derivation, and, ordinarily, the Forest Fire coefficients would be redetermined any time it is changed. Results presented here, comparing shock initiation computations for the quadratic Hugoniot with those for the linear Hugoniot, however, are for the original Forest Fire rate law since the intent is to examine the effects of the amount of reaction associated with the shock only.

The results of computations made for sustained-shock loading are shown in Figures 14 and 15. The pressure histories of Figure 14 indicate that use of the quadratic Hugoniot reduces the shock pressure and retards its progress. Most of this effect occurs during the early portions of shock propagation and the run to detonation is essentially unchanged. The Pop plot, as shown in Figure 15, is only minimally altered with generally shorter runs to detonation.

In the case of pulsed-shock loading, a more substantial change in the results is noted as shown in Figure 16. The principal effect is to alter the slope of the critical velocity curve such that it is much closer to the experimental value. The general level of agreement is still poor.

As previously noted, the sensitivity of Forest Fire predictions to changes in the amount of reaction in the shock wave is relevant to the use of artificial viscosity in conjunction with the reaction rate law in order to describe reactive shock waves. This appears to produce less reaction than associated with the linear reactive Hugoniot. In the 2DE code, the amount of reaction has been increased by adding the artificial viscous stress to the pressure for purposes of computing the reaction rate.

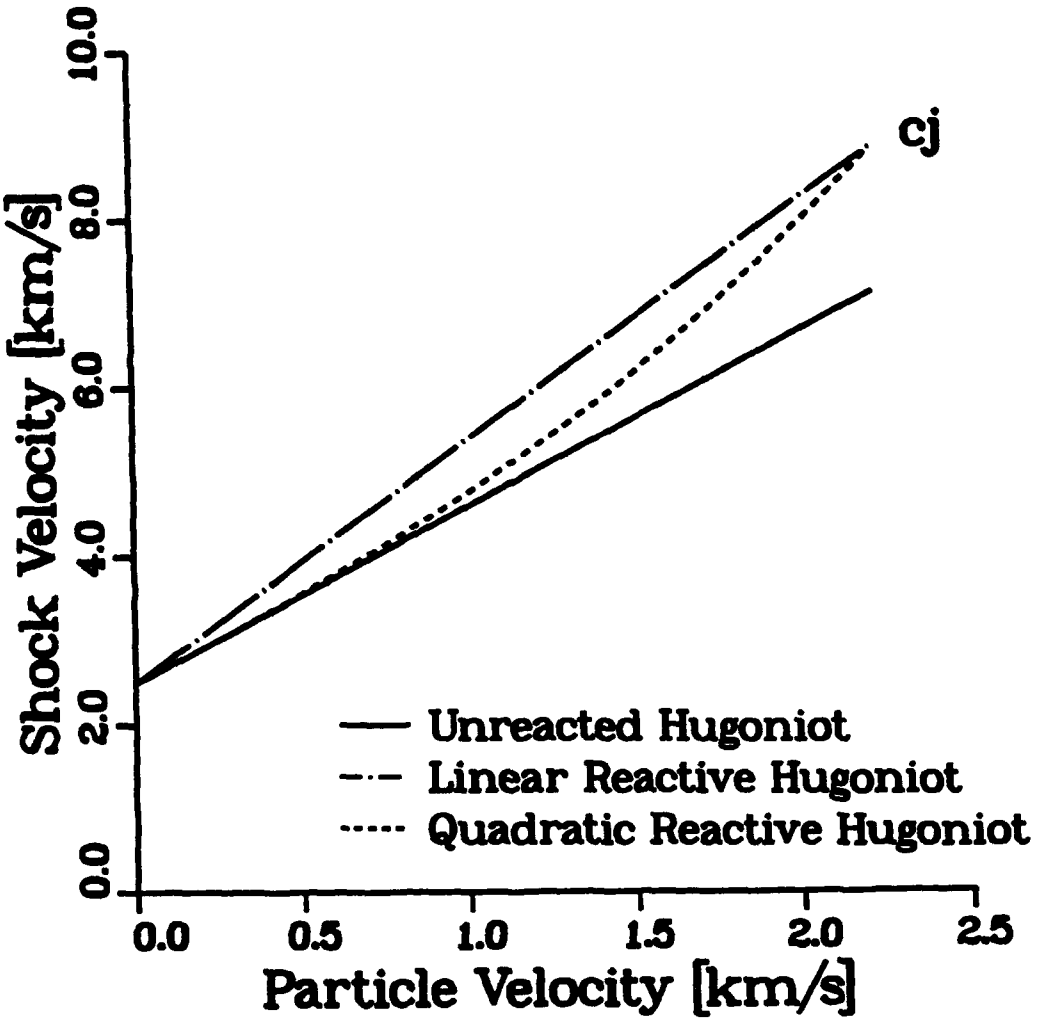

Figure 13. Unreacted and linear and quadratic reactive Hugoniots for PBX-9404. Higher order Hugoniots depart gradually from the inert response at the low velocity end.

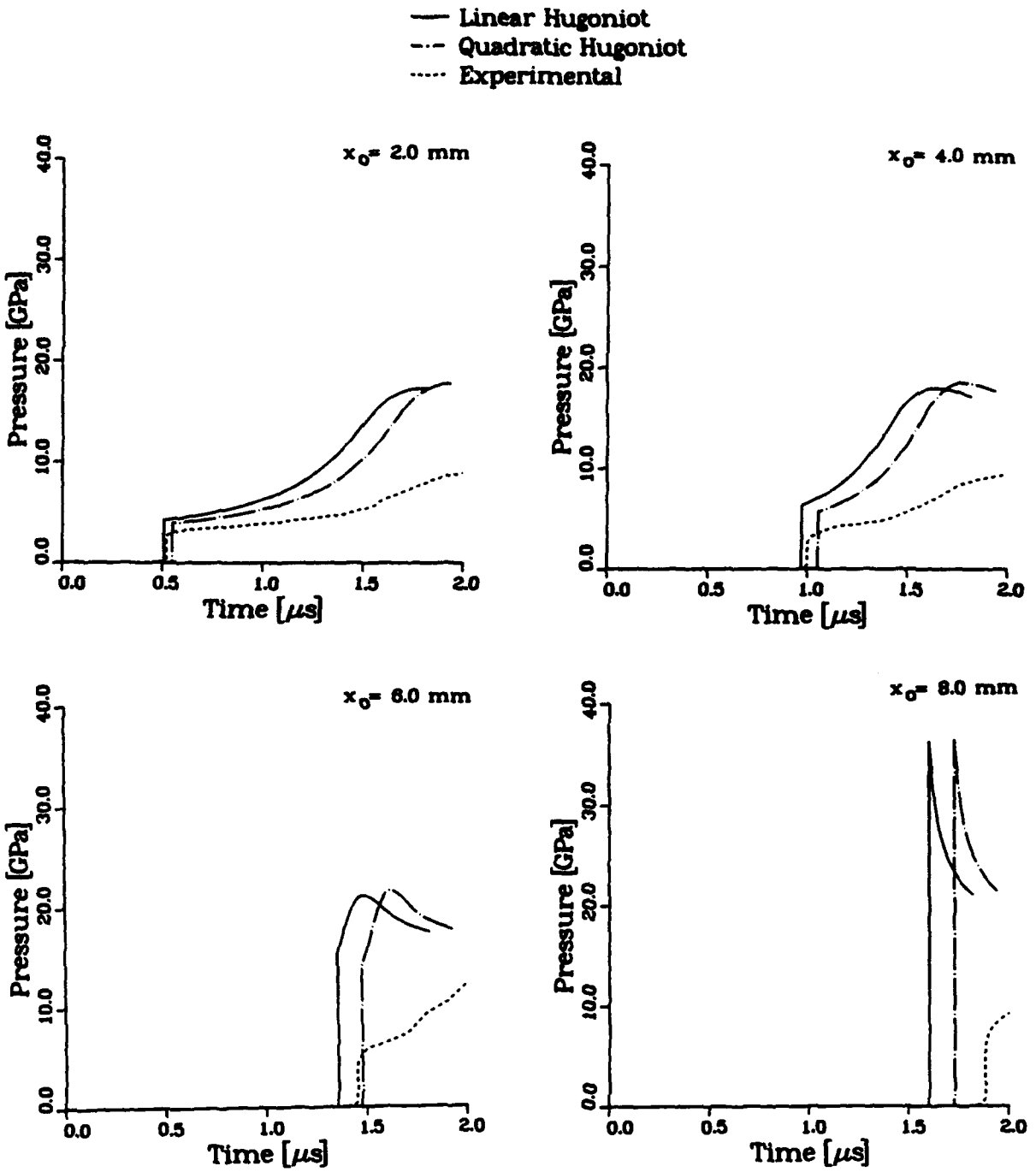

Figure 14. Effect of the reactive Hugoniot order on the predicted pressure histories in a PBX-9404 sample at four Lagrangian stations following the impact of a thick copper flyer at 550 m/s. The results differ only slightly.

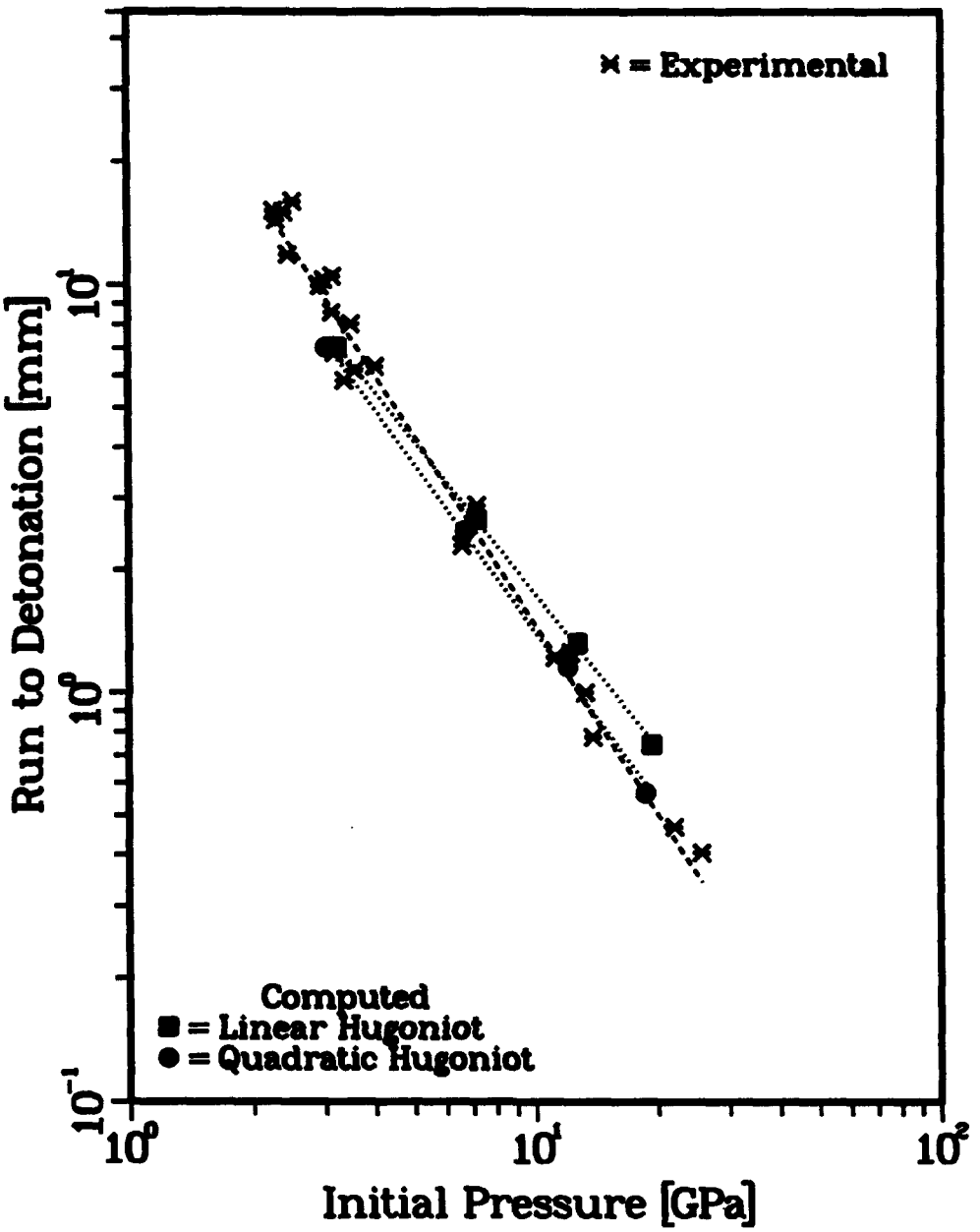

Figure 15. Effect of the reactive Hugoniot order on the predicted Pop plot of PBX-9404. The Pop plot is shifted toward slightly shorter runs at high initial pressures with the quadratic Hugoniot.

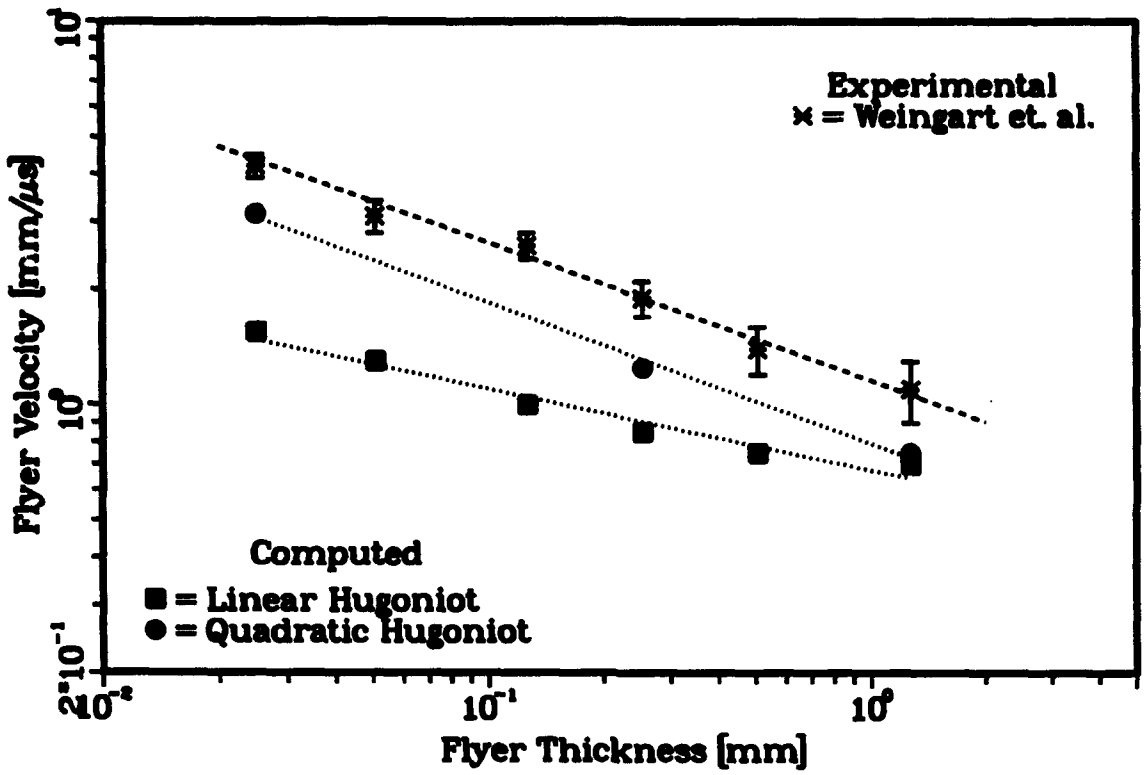

Figure 16. Effect of the reactive Hugoniot order on critical flyer velocities for initiation of PBX-9404 samples by thin mylar flyers. The slope of the predicted critical velocity curve is close to that of the experimental curve.

5.3 Reaction Topology Modeling. The Forest Fire reaction rate model is consistent with bulk reaction. The reaction rate is given by

$$\dot{y}(y,p) = (1-y)F(p) \quad ,$$

where product mass fraction, y, is used to characterize reaction progress and $F(p)$ is the Forest Fire pressure fit. The reaction rate may be generalized as the product of function of mass fraction and a function of pressure.

$$\dot{y}(y,p) = S(y)F(p) \quad .$$

Considerable research (Howe et al. 1976; Wackerle and Anderson 1984) points to the presence of surface burning mechanisms originating at hot spots which delay the onset of significant reaction after shock passage. Applicability to pulsed-shock loading problems may be improved by adding surface area dependence to the reaction rate model. The surface area dependence may be identified with the mass-fraction dependent function while the original pressure dependence is retained. A simplification of a previously proposed surface area model (Starkenberg 1989) may be readily applied to the generalized form of the Forest Fire rate law. In this case,

$$S(y) = A \begin{cases} (y/y_t)^{2/3} & 0 \le y \le y_t \\ [(1-y)/(1-y_t)]^{2/3} & y_t \le y \le 1 \end{cases} .$$

This model is consistent with transition from outward "hole burning" to inward "grain burning" at a point specified by a single calibration parameter, y_t, referred to as the "transition mass fraction." Small values of y_t imply early transition to grain burning. This parameter can be set with reference to available pulsed-shock response data. The leading coefficient, A, is determined by equating the integral of the surface area function with respect to mass fraction to the similar integral of the Forest Fire bulk reaction model. This gives A=5/6, and is intended to help ensure that the sustained-shock response of the model is not significantly altered. The surface area function has been plotted for two values of y_t, and is compared with the bulk reaction function in Figure 17. The function most closely conforms to bulk

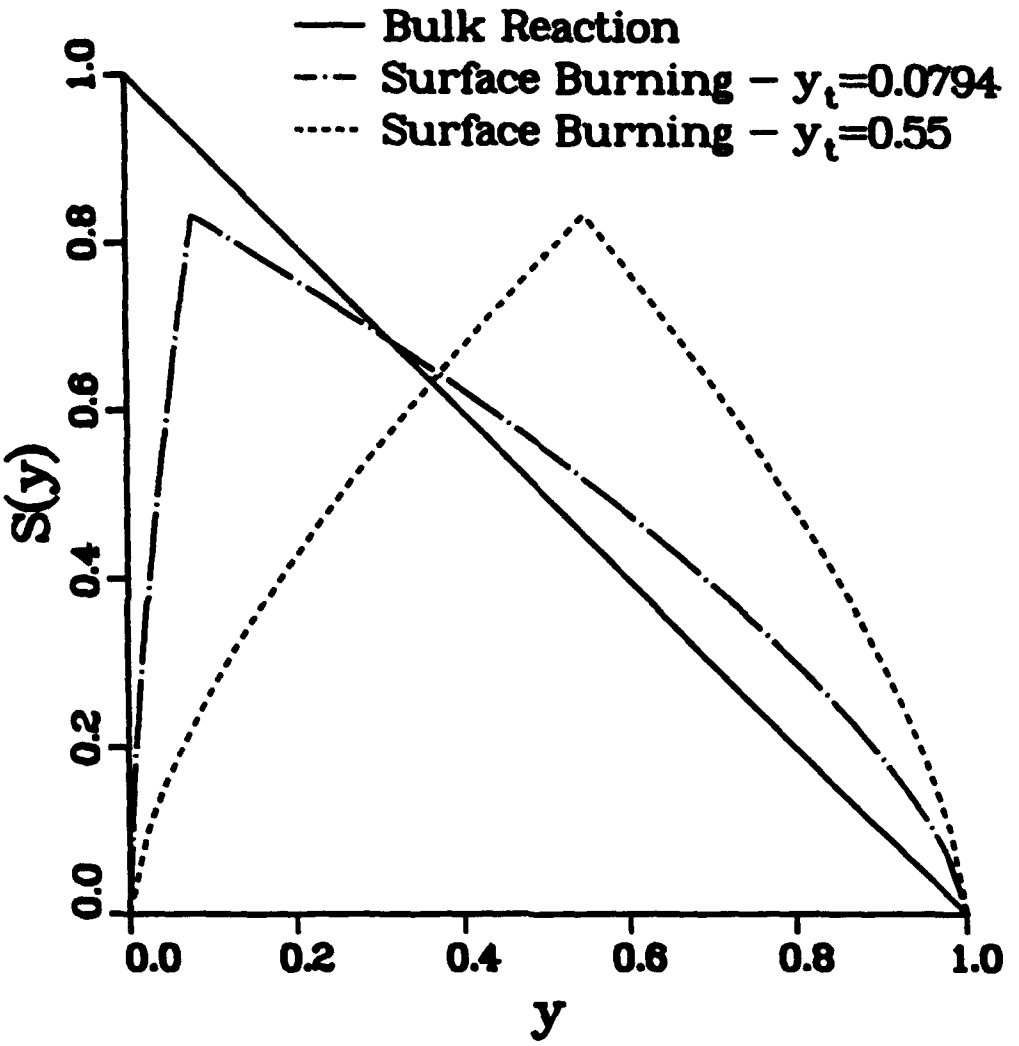

Figure 17. Comparison of bulk and surface reaction functions. Low transition mass fractions produce closer conformity to the bulk reaction function.

reaction for small values of the transition mass fraction. Since the surface area (and, hence, the reaction rate) vanishes for unreacted explosive, this model cannot be used in conjunction with ramp-wave loading unless an ignition model is supplied.

Using y_t, the surface burning model was calibrated to reproduce the experimental critical flyer velocity at a flyer thickness of 0.254 mm. This lies at the middle of the range of flyer thicknesses considered. In conjunction with the linear reactive Hugoniot, the calibration gives y_t=0.55. Results for the thinnest and thickest flyers, as well as the 0.254-mm flyer, are shown in Figure 18. The principal effect on the critical velocity curve is to translate it toward higher critical velocities as the transition mass fraction increases. Thus, away from the calibration point, agreement with experimental data is poor.

Comparison of the pressure histories for sustained-shock loading is shown in Figure 19. Transition to detonation occurs beyond the last station. The effect on the Pop plot, as shown in Figure 20, is substantial. This is primarily due to the relatively large value of y_t, which produces a large delay in the onset of significant reaction following shock passage. The run to detonation associated with the lowest initial pressure lies beyond the limits of the plot, and was deemed too long to compute. Equating the area under the surface area function to that under the bulk reaction function did not successfully preserve the Pop plot for the value y_t of used. The pressure profiles in Figure 21 for copper flyer impact at 1,000 m/s show that transition to detonation occurs by means of an overtaking reaction-driven compression rather than a growing square wave. This is also due to the reaction delay associated with the surface area mechanism.

5.4 Combined Modifications. The use of different reactive Hugoniots was seen to rotate the critical velocity curve while the use of the surface area model in conjunction with different values of transition mass fraction was shown to translate it. It appears that improved agreement with experimental data might be achieved by combining these two modifications.

Another calibration of the surface area model using the quadratic reactive Hugoniot gives y_t=0.0794. This produces substantially better results for pulsed-shock response, as shown in Figure 22. It appears that a still higher order Hugoniot and smaller transition mass fraction would provide further improvement. It is notable that the best results are achieved with a very small value of the transition mass fraction corresponding to a very early transition to grain burning.

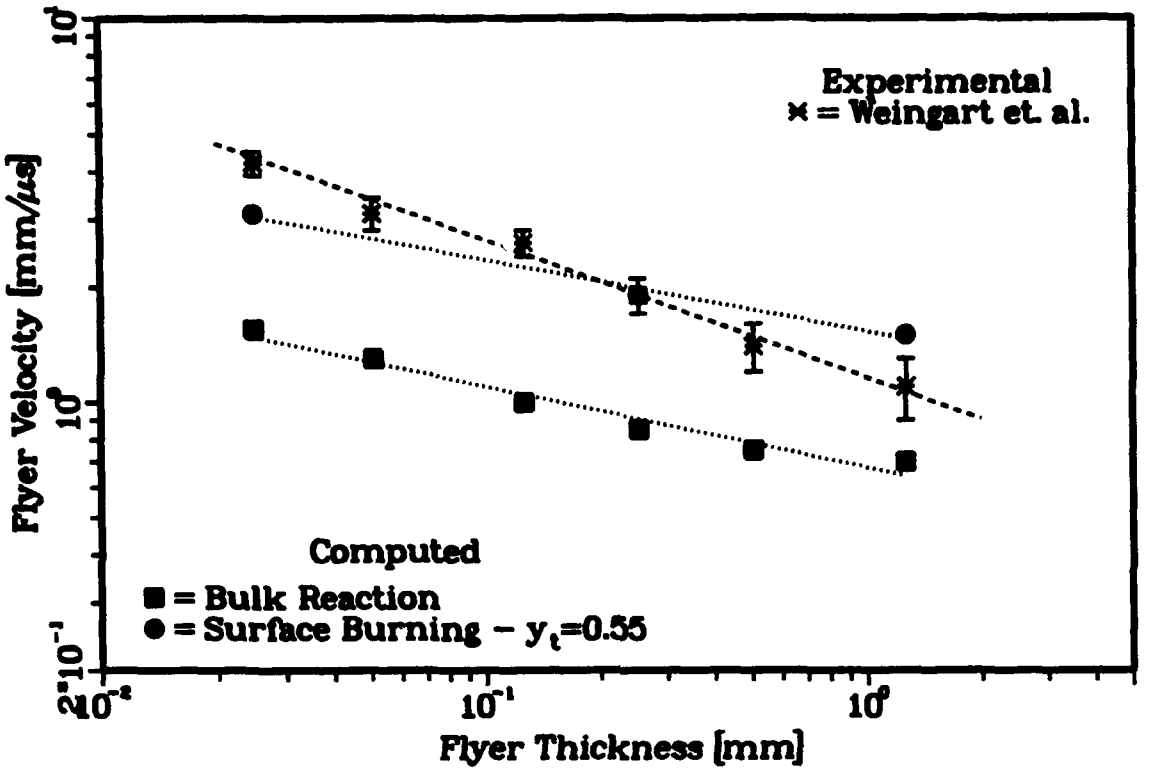

Figure 18. Effect of reaction topology on critical flyer velocities for initiation of PBX-9404 samples by thin mylar flyers. The transition mass fraction has been calibrated at y_t=0.55 to produce agreement with the experiments for a flyer thickness of 0.254 mm. The slope of the predicted critical velocity curve is not close to that of the experimental curve.

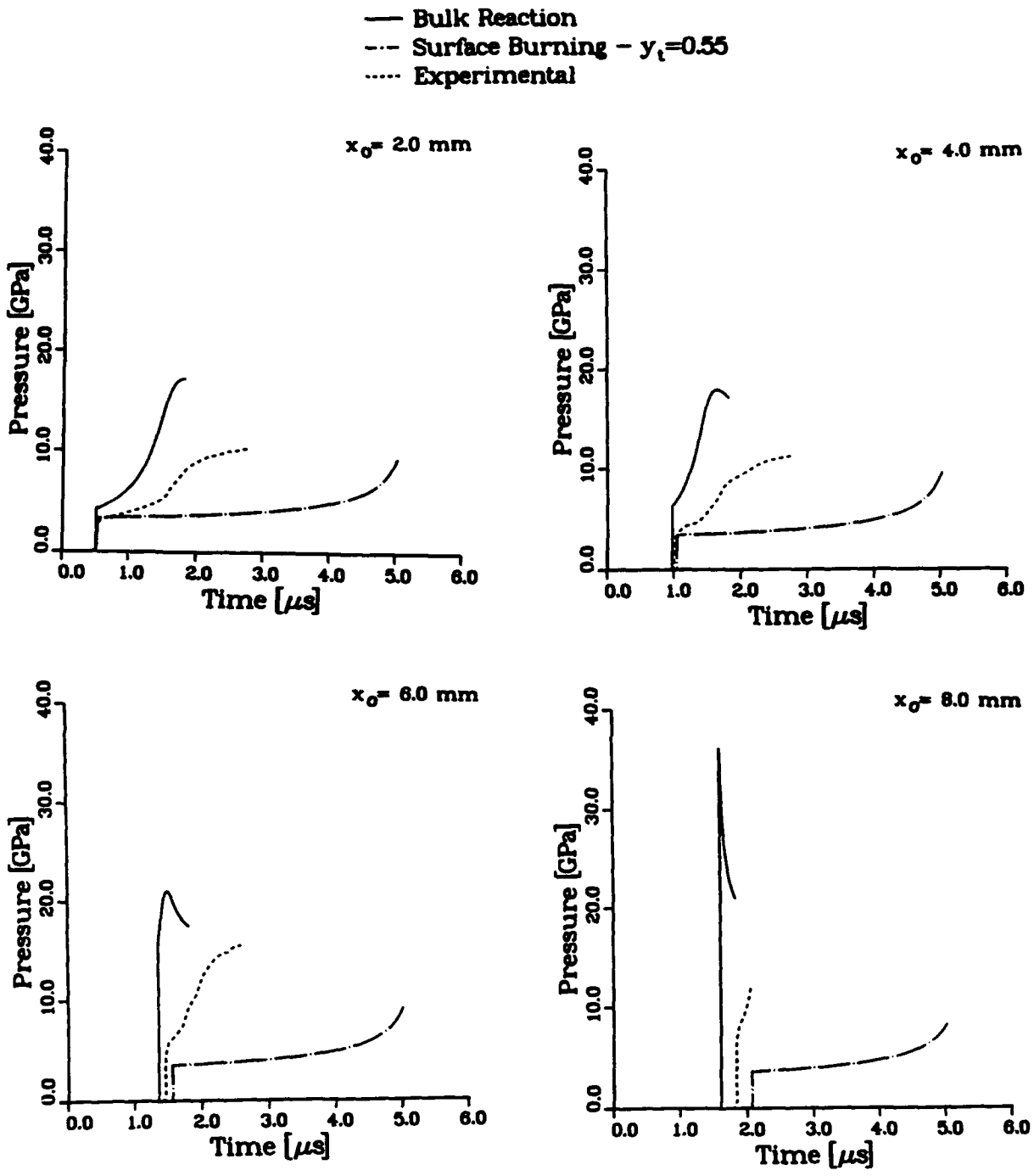

Figure 19. Effect of reaction topology on the predicted pressure histories in a PBX-9404 sample at four Lagrangian stations following the impact of a thick copper flyer at 550 m/s. Surface burning with y_t=0.55 produces a substantial delay in the onset of significant reaction following shock passage.

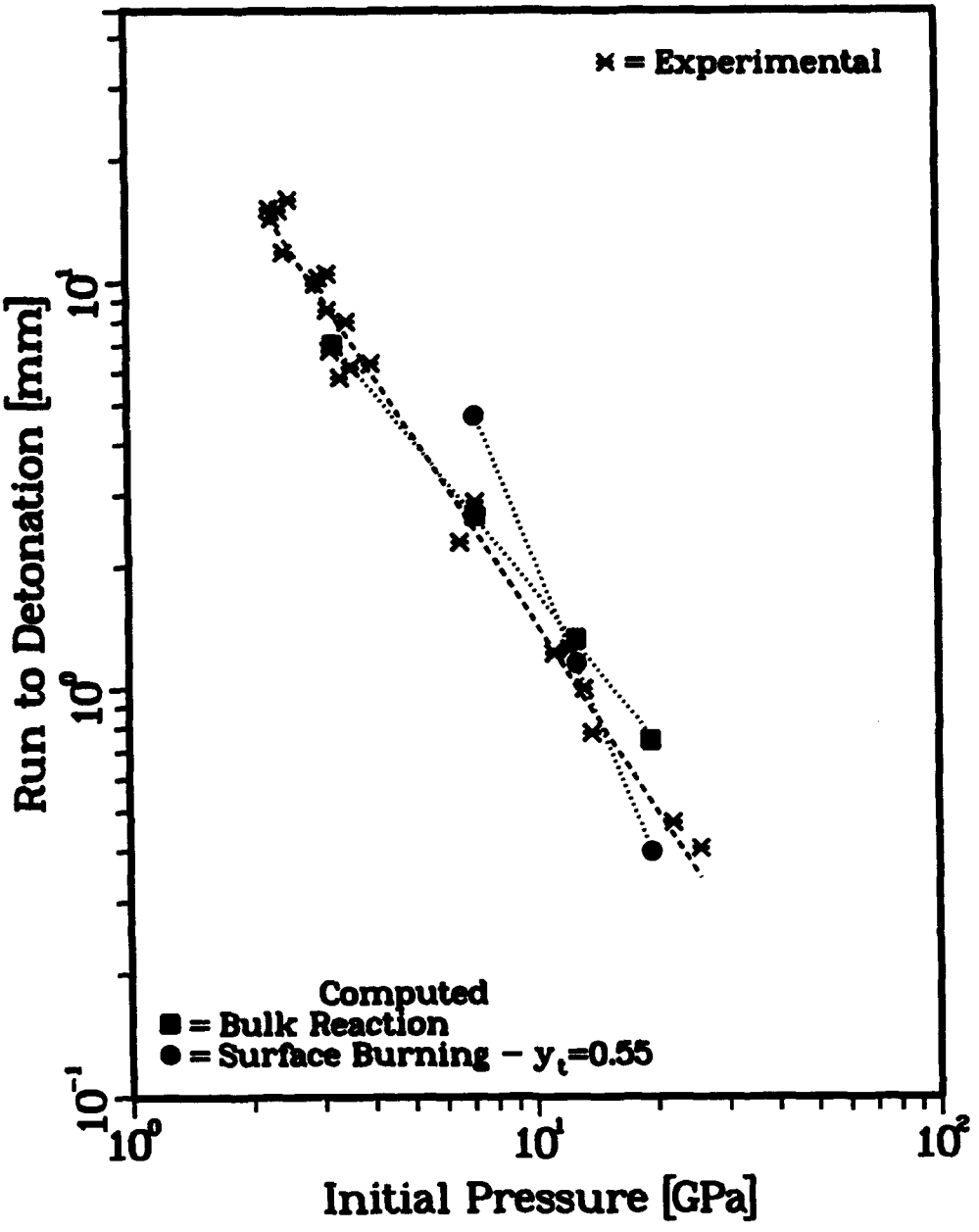

Figure 20. Effect of reaction topology on the predicted Pop plot of PBX-9404. The slope of the Pop plot is substantially altered using surface burning with y_t=0.55.

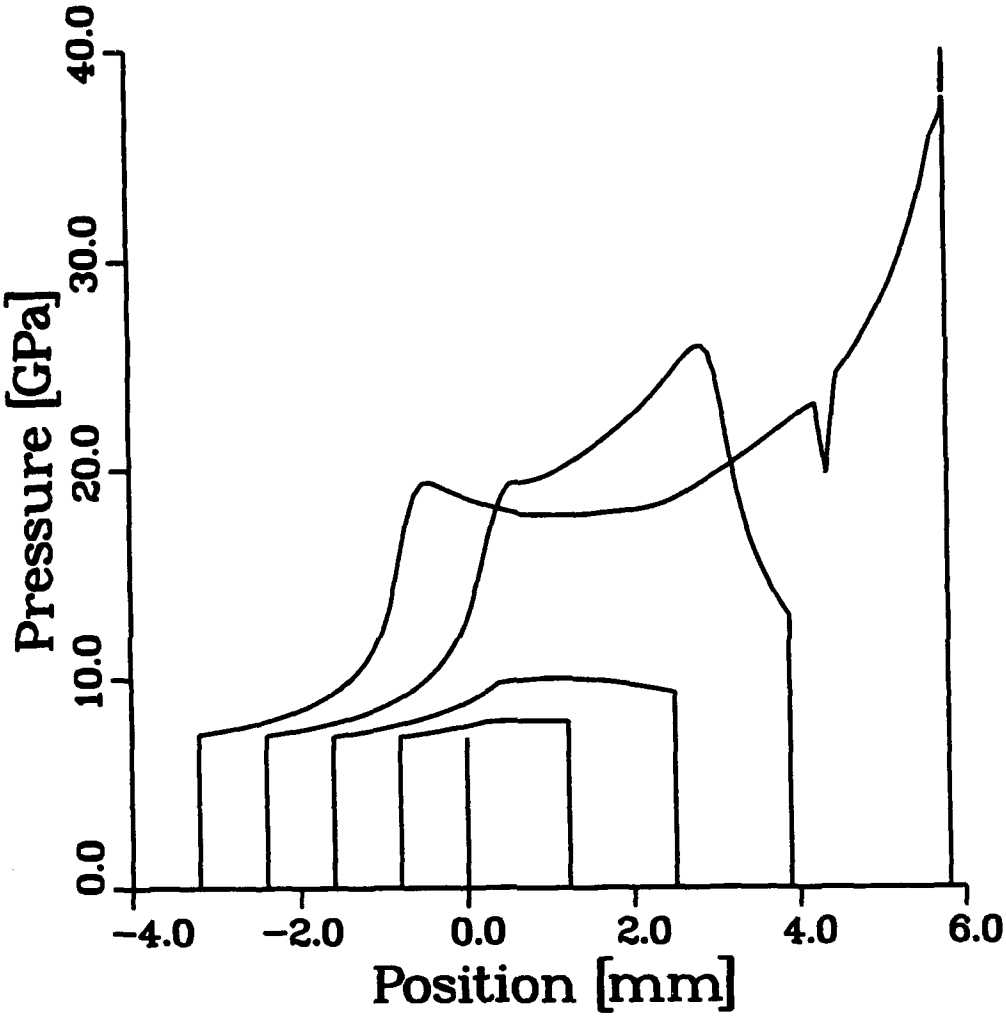

Figure 21. Sequence of pressure profiles showing detonation development in a PBX-9404 sample following the impact of a thick copper flyer at 1,000 m/s using surface burning with y_s=0.55. The shock-wave transitions to detonation on being overtaken by a reaction-driven compression wave, and not as a growing square wave.

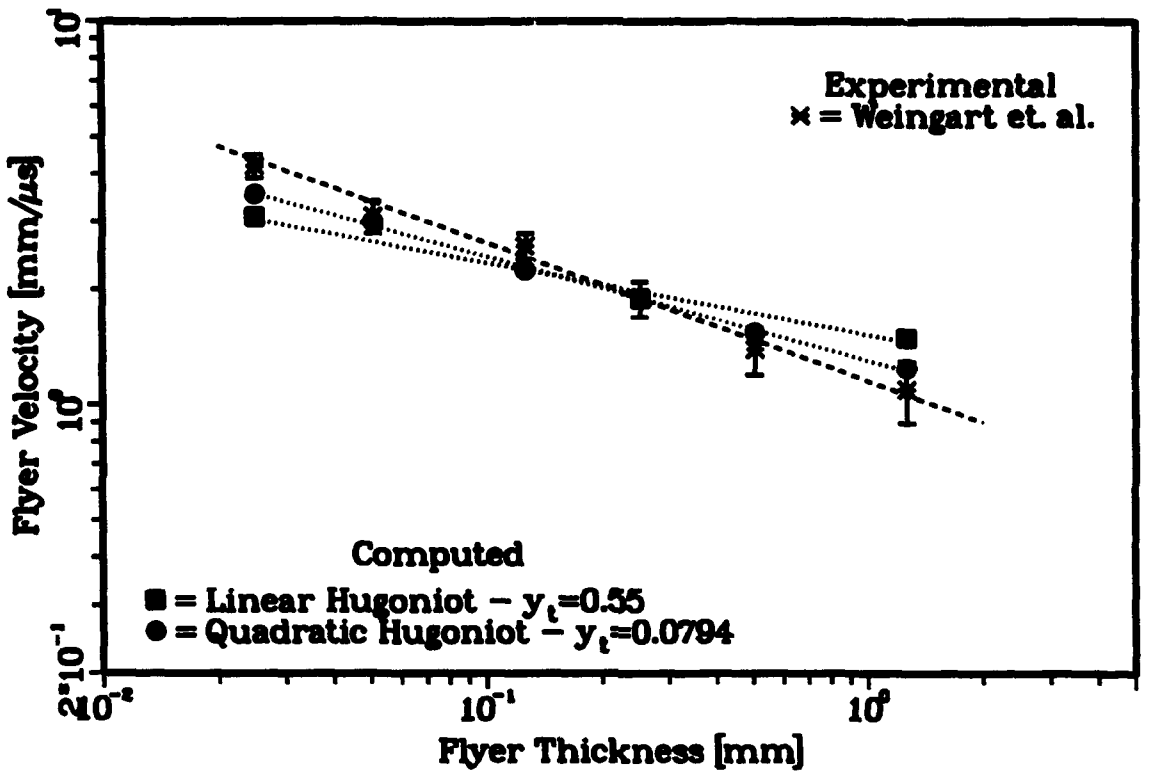

Figure 22. Effect of combining a quadratic reactive Hugoniot with surface burning on critical flyer velocities for initiation of PBX-9404 samples by thin mylar flyers. The transition mass fraction has been calibrated at y_t =0.0794 to produce agreement with the experiments for a flyer thickness of 0.254 mm. The slope of the predicted critical velocity curve is closer to that of the experimental curve.

The effect on the Pop plot is shown in Figure 23. The improved agreement with experiment is attributable to closer conformity to the bulk reaction model when using small values of use of y_r. The fact that agreement with experiment is improved with respect to that achieved using the original Forest Fire model may be regarded as fortuitous.

The effect on the prediction of gauge data for sustained-shock loading is shown in Figure 24. The comparison is still not favorable. The amount of reaction in the shock wave has been reduced but the reaction delay following shock passage appears too great. The presence of a strong compression wave overtaking the initial shock is evident.

6. SUMMARY

Forest Fire is limited in its applicability beyond prediction of run to detonation for sustained-shock loading. The reactive flow field is inadequately represented, even in this case. Forest Fire's prediction of response to pulsed-shock loading is grossly in error. Some aspects of the predicted response to ramp-wave loading are qualitatively correct but there is no reason to believe that Forest Fire can be accurately applied in this case.

The assumption of adiabatic reaction (or isentropic reactants) is more physically realistic than that of thermal equilibrium. The effect of this assumption on flow field prediction may be substantial, especially in the case of pulsed-shock loading. Implementation of adiabatic reaction through the energy conservation equations is an economical computational approach.

Reaction occurring within the shock wave constitutes Forest Fire's ignition model. The amount of such reaction is determined either by integration of the reaction rate law through a viscous shock or by use of a reactive Hugoniot in conjunction with an explicit shock model. The influence of the ignition reaction on the response to pulsed-shock loading is significant.

The inclusion of a surface burning model also has a profound effect on the computational results. When combined with the quadratic reactive Hugoniot, it provides a good representation of the responses to a pulsed-shock stimulus. The best results are achieved with calibration corresponding to a very early transition to grain burning.

The effects of modifications to Forest Fire are most significant with respect to the predicted response to pulsed shock waves. Each of the modifications considered produced large changes in the critical impact velocities for thin flyers. The effects on the Pop plot, except in the case of surface burning, are not significant.

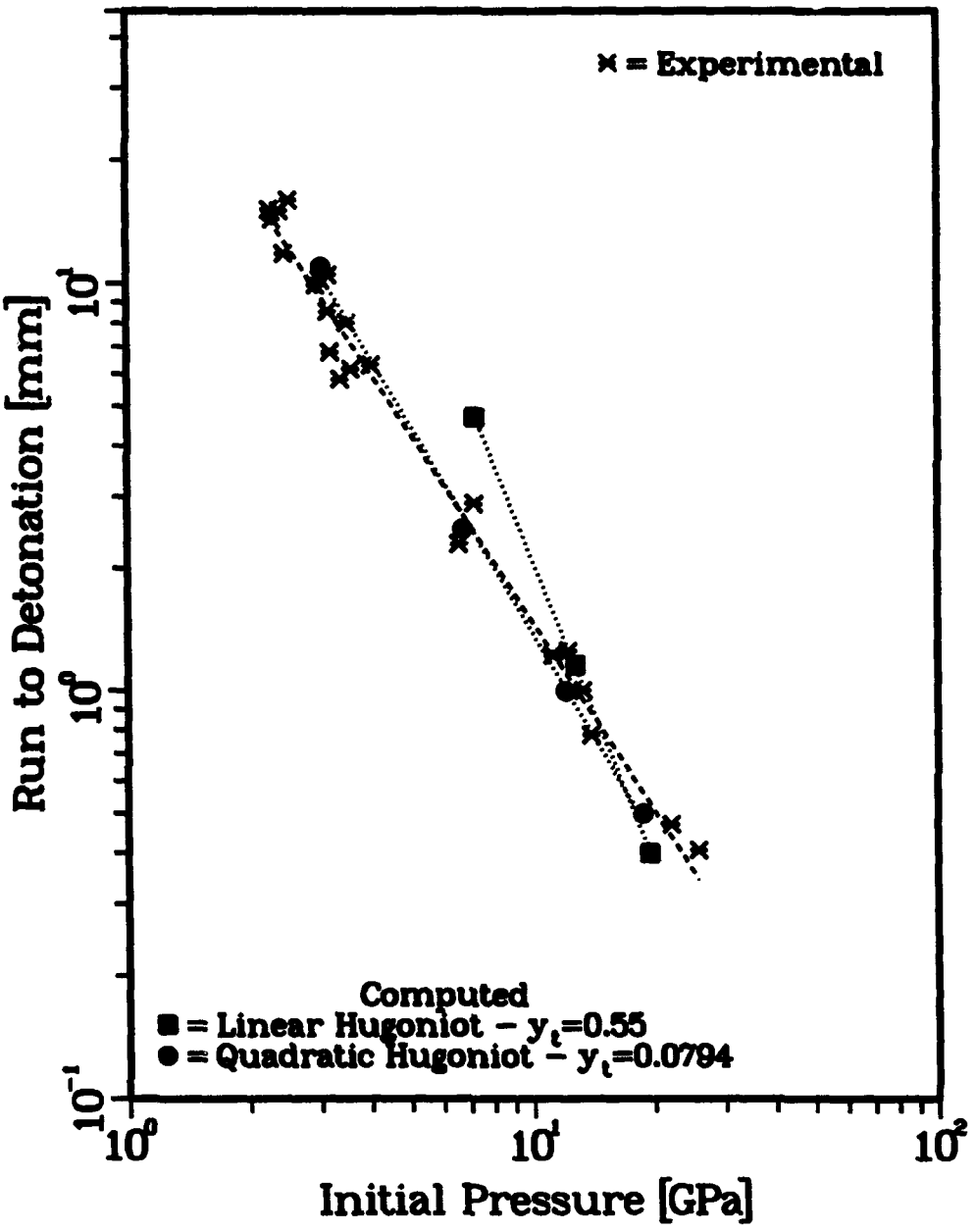

Figure 23. Effect of combining a quadratic reactive Hugoniot with surface burning on the predicted Pop plot of PBX-9404. The predicted Pop plot conforms more closely to the experimental plot using the quadratic Hugoniot and surface burning with y_t=0.0794 than it does using the original Forest Fire assumptions.

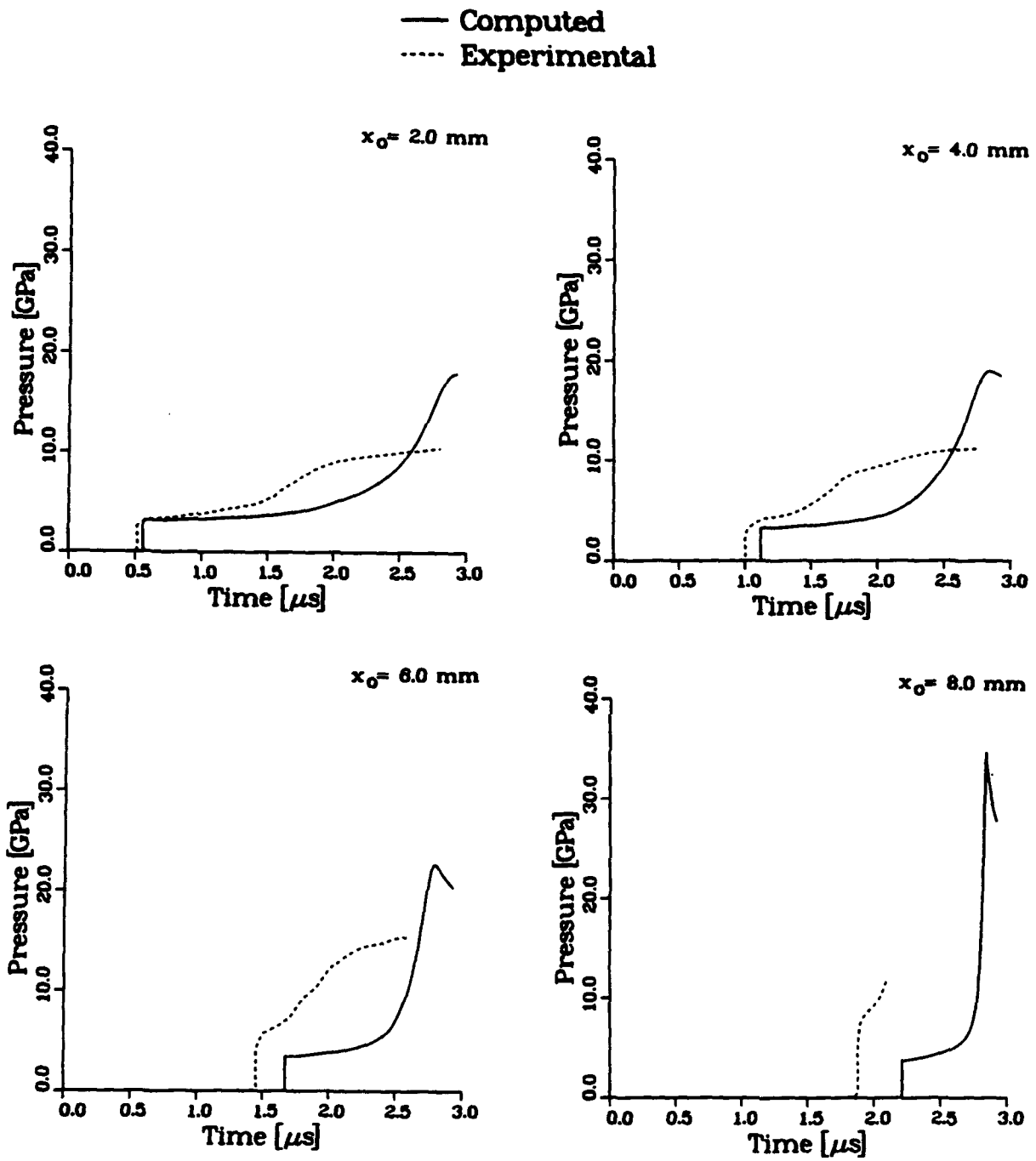

Figure 24. Comparison of experimental pressure histories with Forest Fire predictions at four Lagrangian stations following the impact of a thick copper flyer on a PBX-9404 sample at 550 m/s using the quadratic Hugoniot and surface burning with y_r=0.0794. The amount of reaction in the shock wave has been reduced but the reaction delay following shock passage appears too great.

7. REFERENCES

Bowman, A. L., C. A. Forest, J. D. Kershner, C. L. Mader, and G. H. Pimbley. "Numerical Modeling of Shock Sensitivity Experiments." Proceedings of the Seventh Symposium (International) on Detonation, pp. 479–487, 1981.

Cost, T. L., W. B. Thomas, S. L. Vance, and D. J. Jones. "Bullet and Fragment Impact Testing and Analysis for the Army IM Database." Proceedings of the 1992 JANNAF Propulsion Systems Hazards Subcommittee Meeting, pp. 227–235, 1992.

Gibbs, T. R., and A. Popolato (editors). LASL Explosive Property Data. Berkeley: University of California Press, 1980.

Howe, P. M., R. B. Frey, B. C. Taylor, and V. M. Boyle. "Shock Initiation and the Critical Energy Concept." Proceedings of the Sixth Symposium (International) on Detonation, pp. 11–19, 1976.

Johnson, J. N., P. K. Tang, and C. A. Forest. "Shock Wave Initiation of Heterogeneous Reactive Solids." Journal of Applied Physics, vol. 57, no. 9, 1985.

Kershner, J. D., and C. L. Mader. "2DE, A Two-Dimensional Continuous Eulerian Hydrodynamic Code for Computing Multicomponent Reactive Hydrodynamic Problems." LA-4846, Los Alamos Scientific Laboratory, Los Alamos, NM, 1972.

Lee, E. L., and C. M. Tarver. "Phenomenological Model of Shock Initiation in Heterogeneous Explosives." Physics of Fluids, vol. 23, no. 12, pp. 2362–2372, 1980.

Lundstrom, E. A. "Evaluation of Forest Fire Burn Model of Reaction Kinetics of Heterogeneous Explosives." Naval Weapons Center Technical Publication 6898, China Lake, CA 1988.

Mader, C. L. "An Empirical Model of Heterogeneous Shock Initiation of 9404." LA-4475, Los Alamos Scientific Laboratory, Los Alamos, NM, 1970.

Mader, C. L. Numerical Modeling of Detonation. Berkeley: University of California Press, 1979.

Mader, C. L., and C. A. Forest. "Two Dimensional Homogeneous and Heterogeneous Detonation Wave Propagation." LA-6259, Los Alamos Scientific Laboratory, Los Alamos, NM, 1976.

Ramsay, J. B., and A. Popolato. "Analysis of Shock Wave and Initiation Data for Solid Explosives." Proceedings of the Fourth Symposium (International) on Detonation, pp. 233–238, 1965.

Setchell, R. E. "Ramp-Wave Initiation of Granular Explosives." Combustion and Flame, vol. 43, pp. 255–264, 1981.

Starkenberg, J. "A Model for the Initiation of Heterogeneous High Explosives Subject to General Compressive Loading." Proceedings of the Ninth Symposium (International) on Detonation, pp. 604–617, 1989.

Starkenberg, J., T. M. Dorsey, K. J. Benjamin, and A. L. Arbuckle. "A Computational Assessment of the Role of Shielding in Preventing the Sympathetic Detonation of Munitions." Proceedings of the Ninth Symposium (International) on Detonation, pp. 1489–1501, 1989.

Starkenberg, J., Y. K. Huang, and A. L. Arbuckle. "Numerical Modeling of Projectile Impact Shock Initiation of Bare and Covered Composition B." ARBRL-TR-02576, U.S. Army Ballistic Research Laboratory, Aberdeen Proving Ground, MD, 1984.

Tang, P. K., J. N. Johnson, and C. A. Forest. "Modeling Heterogeneous High Explosive Burn with an Explicit Hot Spot Process." Proceedings of the Eighth Symposium (International) on Detonation, pp. 52–61, 1985.

Wackerle, J., R. L. Rabie, M. J. Ginsberg, and A. B. Anderson. "A Shock Initiation Study of PBX-9404." Symposium on High Dynamic Pressures, Paris, 1978.

Wackerle, J., and A. B. Anderson. "Burning Topology in the Shock-Induced Reaction of Heterogeneous Explosives." Shock Waves in Condensed Matter. Edited by J. R. Asay, R. A. Graham, G. K. Straub Elsevier Science Publishers B. V., 1984.

Weingart, R. C., R. K. Jackson, C. A. Honodel, and R. S. Lee. "Shock Initiation of PBX-9404 by Electrically Driven Flyer Plates." Propellants and Explosives, vol. 5, pp. 158–162, 1980.

No. of Copies	Organization
2	Administrator Defense Technical Info Center ATTN: DTIC-DDA Cameron Station Alexandria, VA 22304-6145
1	Commander U.S. Army Materiel Command ATTN: AMCAM 5001 Eisenhower Ave. Alexandria, VA 22333-0001
1	Director U.S. Army Research Laboratory ATTN: AMSRL-OP-CI-AD, Tech Publishing 2800 Powder Mill Rd. Adelphi, MD 20783-1145
1	Director U.S. Army Research Laboratory ATTN: AMSRL-OP-CI-AD, Records Management 2800 Powder Mill Rd. Adelphi, MD 20783-1145
2	Commander U.S. Army Armament Research, Development, and Engineering Center ATTN: SMCAR-TDC Picatinny Arsenal, NJ 07806-5000
1	Director Benet Weapons Laboratory U.S. Army Armament Research, Development, and Engineering Center ATTN: SMCAR-CCB-TL Watervliet, NY 12189-4050
1	Director U.S. Army Advanced Systems Research and Analysis Office (ATCOM) ATTN: AMSAT-R-NR, M/S 219-1 Ames Research Center Moffett Field, CA 94035-1000

No. of Copies	Organization
1	Commander U.S. Army Missile Command ATTN: AMSMI-RD-CS-R (DOC) Redstone Arsenal, AL 35898-5010
1	Commander U.S. Army Tank-Automotive Command ATTN: AMSTA-JSK (Armor Eng. Br.) Warren, MI 48397-5000
1	Director U.S. Army TRADOC Analysis Command ATTN: ATRC-WSR White Sands Missile Range, NM 88002-5502
(Class. only) 1	Commandant U.S. Army Infantry School ATTN: ATSH-CD (Security Mgr.) Fort Benning, GA 31905-5660
(Unclass. only) 1	Commandant U.S. Army Infantry School ATTN: ATSH-WCB-O Fort Benning, GA 31905-5000
1	WL/MNOI Eglin AFB, FL 32542-5000
	Aberdeen Proving Ground
2	Dir, USAMSAA ATTN: AMXSY-D AMXSY-MP, H. Cohen
1	Cdr, USATECOM ATTN: AMSTE-TC
1	Dir, ERDEC ATTN: SCBRD-RT
1	Cdr, CBDA ATTN: AMSCB-CII
1	Dir, USARL ATTN: AMSRL-SL-I
5	Dir, USARL ATTN: AMSRL-OP-CI-B (Tech Lib)

No. of Copies	Organization
1	Wright Laboratory Armament Directorate ATTN: J. Gregory Glenn Egline Air Force Base, FL 32542-5434
2	Naval Surface Warfare Center ATTN: Richard Bernecker Kibong Kim 10901 New Hampshire Ave. Silver Spring, MD 20903-5640
6	Los Alamos National Laboratory ATTN: Alan L. Bowman Charles A. Forest James N. Johnson Edward M. Kober Pier K. Tang Jerry Wackerle Los Alamos, NM 87545
1	Los Alamos National Laboratory ATTN: Phillip M. Howe P.O. Box 1663 Los Alamos, NM 87545
2	Sandia National Laboratories ATTN: G. I. Kerley Robert E. Setchell P.O. Box 5800 Albuquerque, NM 87185-5800
3	Lawrence Livermore National Laboratory ATTN: Edward L. Lee Michael J. Murphy Craig M. Tarver P.O. Box 808 Livermore, CA 94550
1	Naval Air Warfare Center ATTN: Eric A. Lundstrom China Lake, CA 93555
1	New Mexico Institute of Mining Technology ATTN: Larry D. Libersky Campus Station Socorro, NM 87801

No. of Copies	Organization
1	Vanderbilt University ATTN: Arthur M. Mellor Box 1592 Nashville, TN 37235-1592
1	Dyna East Corporation ATTN: Pei Chi Chou 3201 Arch St. Philadelphia, PA 19104
	ABERDEEN PROVING GROUND
11	Dir, USARL ATTN: AMSRL-WT-TB, Kelly J. Benjamin Vincent M. Boyle Toni M. Dorsey Robert B. Frey Fred Gregory Warren Hillstrom William Lawrence Ona Lyman Evelyn McDougal Jerry Watson AMSRL-WT-PE, Douglas E. Kooker

No. of Copies	Organization
1	DGA/Centre d'Etudes de Gramat ATTN: Didier Bergues Gramat, 46500, FRANCE
1	Commissariate a l'Energie Atomique ATTN: Jean-Paul Plotard Courtry, 77181, FRANCE
1	French-German Research Institute (ISL) ATTN: Michel M. S. Samirant 5 Rue de General Cassagnou Saint-Louis Cedex, 68301, FRANCE
1	ICI Explosives ATTN: David L. Kennedy P.O. Box 196 George Booth Dr. New South Wales, 2327, AUSTRALIA
1	Agency For Defense Development ATTN: Jaimin Lee Yuseong P.O. Box 35 (1-3-7) Taejon, 305-600, KOREA

INTENTIONALLY LEFT BLANK.

USER EVALUATION SHEET/CHANGE OF ADDRESS

This Laboratory undertakes a continuing effort to improve the quality of the reports it publishes. Your comments/answers to the items/questions below will aid us in our efforts.

1. ARL Report Number ARL-TR-373 Date of Report March 1994

2. Date Report Received _____

3. Does this report satisfy a need? (Comment on purpose, related project, or other area of interest for which the report will be used.) _____

4. Specifically, how is the report being used? (Information source, design data, procedure, source of ideas, etc.) _____

5. Has the information in this report led to any quantitative savings as far as man-hours or dollars saved, operating costs avoided, or efficiencies achieved, etc? If so, please elaborate. _____

6. General Comments. What do you think should be changed to improve future reports? (Indicate changes to organization, technical content, format, etc.) _____

CURRENT ADDRESS

_____
Organization

_____
Name

_____
Street or P.O. Box No.

_____
City, State, Zip Code

7. If indicating a Change of Address or Address Correction, please provide the Current or Correct address above and the Old or Incorrect address below.

OLD ADDRESS

_____
Organization

_____
Name

_____
Street or P.O. Box No.

_____
City, State, Zip Code

(Remove this sheet, fold as indicated, tape closed, and mail.)
(DO NOT STAPLE)

DEPARTMENT OF THE ARMY

OFFICIAL BUSINESS

BUSINESS REPLY MAIL
FIRST CLASS PERMIT No 0001, APG, MD

Postage will be paid by addressee.

Director
U.S. Army Research Laboratory
ATTN: AMSRL-OP-CI-B (Tech Lib)
Aberdeen Proving Ground, MD 21005-5066

NO POSTAGE
NECESSARY
IF MAILED
IN THE
UNITED STATES